COMPARATIVE ANALYSIS OF THE CHARACTERISTICS OF PROMISING APSK MODULATION SCHEMES IN WIRELESS TELECOMMUNICATIONS

DOI: 10.36724/2072-8735-2025-19-9-59-76

Gennady N. Kazakov,
Moscow Aviation Institute (National Research University), Moscow, Russia, ***jee2@mail.ru***

Nguyen Huy Tung,
Moscow Aviation Institute (National Research University), Moscow, Russia, ***nguyenhuytung201@gmail.com***

Timofey Ya. Shevgunov,
Moscow Aviation Institute (National Research University), Moscow, Russia, ***shevgunov@gmail.com***

Evgenii N. Efimov,
Moscow Aviation Institute (National Research University), Moscow, Russia, ***omegatype@gmail.com***

Manuscript received 28 June 2025;
Accepted 30 August 2025

This research has been funded by the grant of the Russian Science Foundation (RSF), no. 25-21-00281, https://rscf.ru/en/project/25-21-00281/.

Keywords: *signals with circular signal constellations, constellation figure of merit (CFM), peak to average power ratio (PAPR), symbol error probability (SEP), irregular HQAM (IHQAM), circular θ-quadrature amplitude modulation (CTQAM), Star QAM, MIL-STD-188-110 standard signals*

The growing requirements for the use of high-speed and energy-efficient high-capacity data transmission channels in modern and future telecommunication networks have led to an increasing interest in the formation and application of signals with new constellations. Requirements for the shape of signal constellations in connection with the emergence of new technologies of wireless telecommunications are formulated. Promising variants of APSK modulation schemes with circular signal constellations have been selected, which include signals with irregular hexagonal quadrature amplitude modulation (IHQAM), signals with circular ?-quadrature amplitude modulation (CTQAM), as well as signals of the Digital Video Broadcast System (DVB) S2X and MIL-STD-188-110 standards. Three metrics were used to compare the performance of APSK signals: Constellation Figure of Merit (CFM), Peak-to-Average Power Ratio (PAPR), and Symbol Error Probability (SEP). Based on the selected metrics, analytical expressions of the quality indicators of the studied signals were obtained and their numerical calculation was carried out. Recommendations are formulated on the expediency of using the studied signals with circular constellations in modern and promising wireless telecommunication networks. To show the correctness of the proposed analytical expressions, some results of accurate computer modeling are presented.

Information about authors:
Gennady N. Kazakov, *PhD, docent of the Department of Theoretical Radio Engineering, Moscow Aviation Institute (National Research University), Moscow, Russia, ORCID 0009-0007-7356-4762*
Nguyen Huy Tung, *student, the Department of Radio electronics, info communications and information security, Moscow Aviation Institute (National Research University), Moscow, Russia, ORCID 0009-0002-5395-4302*
Timofey Ya. Shevgunov, *PhD, docent of the Department of Theoretical Radio Engineering, Moscow Aviation Institute (National Research University), Moscow, Russia, ORCID 0000-0003-1444-983X*
Evgenii N. Efimov, *PhD, engineer of the Department of Theoretical Radio Engineering, Moscow Aviation Institute (National Research University), Moscow, Russia, ORCID 0000-0001-5975-6513*

Для цитирования:
Казаков Г.Н., Нгуен Х.Т., Шевгунов Т.Я., Ефимов Е.Н. Сравнительный анализ характеристик перспективных схем APSK в беспроводных телекоммуникациях // T-Comm: Телекоммуникации и транспорт. 2025. Том 19. №9. С. 59-76.

For citation:
G.N. Kazakov, H.T. Nguyen, T.Y. Shevgunov, E.N. Efimov, "Comparative analysis of the characteristics of promising APSK modulation schemes in wireless telecommunications," *T-Comm*, 2025, vol. 19, no. 9, pp. 59-76.

1 Introduction

At the current stage of the development of wireless telecommunications theory and technology, it is possible to observe the wide development of new areas. These developments are driven by the emergence and growth of new applications, such as the Internet of Things (IoT), remote and intelligent manufacturing, autonomous vehicles, virtual and augmented reality, and high-resolution content delivery. In this regard, the concept of a smart radio environment (SRE) or programmable wireless environments (PWEs) is actively studied and developed to enhance the capabilities of wireless communication networks [1-3].

This concept involves transforming the propagation space in wireless communication systems into a smart, adaptive environment. This environment can dynamically optimize wireless propagation characteristics to improve communication performance, coverage, energy efficiency, and security. Reconfigurable intelligent surfaces (RISs) are used to realize the idea of creating SREs. RISs allow one to change the parameters of electromagnetic waves (phase, amplitude, and polarization) when they interact with the surface. This creates a wireless channel with good characteristics, such as an additive white Gaussian noise (AWGN) channel. This provides guaranteed quality of service (QoS) in telecommunication networks.

Note the current trend of convergence between terrestrial and satellite communication systems. Recently, there has been much attention paid to RF/FSO-based terrestrial-satellite communication systems that use hybrid radiofrequency (RF) and free-space optical (FSO) channels. These systems are described in references [6-8]. There has also been attention paid to RF/FSO communication systems that use radio-frequency intelligent surfaces (RIS). These systems are described in reference [9]. One of the main requirements for future wireless communication systems is the use of energy-efficient, two-dimensional signaling constellations that can provide high performance in channels with different propagation characteristics.

The following main requirements are therefore considered when selecting signal constellations for advanced wireless communication systems and networks.

1. Providing high spectral efficiency by utilizing multi-position APSK.

2. High energy efficiency (by energy efficiency we will mean signals with constellations that provide a given symbol error probability with minimum average power).

3. Providing low peak factor and robustness to nonlinear distortion in satellite channels, as well as maintaining high performance in Additive White Gaussian Noise (AWGN) channels formed using RISs, and in multipath channels with strong fading characteristics of mobile networks.

4. Ability to work with stationary and mobile users, as well as the use of simple methods of demodulation of radio signals.

Provision of the above requirements can be achieved using signals with amplitude-phase modulation (APSK) with optimized shape of signal constellations.

Various existing wireless communication systems and standards, such as ITU, 3GPP, and IEEE, utilize M-ary QAM (M-QAM) constellations to provide high system throughput and spectral efficiency. M-QAM is typically a perfect square for even values of 2m and contains M=2m symbols, where m is the number of bits in the transmitted symbol. Therefore, M-QAM is often referred to as square QAM (SQAM). The advantages of SQAM include the following: first, the SQAM constellation has the maximum possible minimum Euclidean distance between constellation points for a given average symbol power; second, fairly simple maximum likelihood (ML) detection is used to determine the value of the received symbol. However, SQAMs have a rather high peak factor and do not perform well in multipath channels with strong fading, such as the Rayleigh channel.

As is well known, signal constellations based on a hexagonal lattice are the most densely packed and have the highest energy efficiency with limited average power. In this case, signal symbols can be located at the centers of equilateral hexagons and at the vertices of regular triangles. The former is called Hexagonal QAM (HQAM), and the latter is called Triangular Quadrature Amplitude Modulation (TQAM) [10]. However, the boundaries of the 2D partitioning of the signal constellation for symbol value decisions are hexagonal in both cases. Thus, the efficiency of HQAM and TQAM are the same. Theoretically, SQAM, TQAM, and HQAM are special cases of parametric quadrature amplitude modulation (QAM), called θ-QAM. Conversely, as demonstrated in [12], the optimal signal constellation that minimizes error probability under Gaussian noise with bounded average power (given a minimum Euclidean distance) and a high signal-to-noise ratio takes the form of a lattice of equilateral triangles and assumes a circular shape as the number of signal points increases. This has also been confirmed in works on geometric constellation formation based on machine learning, in which symbol detection is performed using neural networks (e.g) [13].

Clearly, APSK with circular constellations has lower peak-to-average power ratio (PAPR) values while maintaining high signal-to-noise ratio (SNR) values. Therefore, this paper will analyze circular signal constellations used in practice and promising signals.

There are several approaches to forming signals with circular constellations. One approach is to create M-ary circular θ-quadrature amplitude modulation (CTQAM) by rearranging the signal points based on θ-QAM. The algorithm for computing the symbol points is given in references [14].

Another way is to transition from regular HQAM (R-HQAM) to irregular HQAM (IHQAM) (optimum). As the number of points in the constellation increases, the IHQAM constellation approaches a circle. The algorithm for generating irregular HQAM is presented in [15]. As will be shown later, the signal constellations obtained by these two methods are quite similar, though not identical. Both approaches preserve the minimum distance between constellation points (given the minimum Euclidean distance). This minimizes the peak-to-average power ratio (PAPR) while providing the best signal-to-noise ratio (SEP).

Another approach is Star QAM, a special case of circular amplitude-phase shift keying (APSK) used in most recent satellite communication standards, such as the Digital Video Broadcasting (DVB) S2 and S2X systems [16, 17]. For these signals, differential detection can be applied instead of coherent detection, eliminating the need for accurate phase tracking and channel estimation during reception. These modulation schemes are also robust to nonlinear distortion in satellite wireless channels.

Finally, the MIL-STD-188-110 standard [18] specifies quadrature modulated signals with quadrature modulation and circular constellations. The modulation scheme specified in this standard is actually a combination of SQAM and PSK.

The purpose of this paper is to compute quality metrics on selected metrics for the listed types of APSK in AWGN channel to provide researchers with a simple analytical apparatus to quantify the performance of signals with different constellations. The remainder of this paper is organized as follows. Section 1 describes the metrics used to compare APSK with different constellations and the study's methodology. It also derives analytical expressions for selected quality metrics and performs computer simulations to validate the correctness of the expressions. Section 2 presents and discusses the main results of the study. Section 3 contains concluding comments.

2 Methods

2.1 Metrics for comparing APSK constellations

We will use three metrics - constellation figure of merit, peak to average power ratio and symbol error probability.

2.1.1 Constellation figure of merit (CFM) [20, 21]

The CFM value is used as a measure to determine how efficiently a constellation utilizes SNR, i.e., it provides a measure of the performance of constellation C. If a constellation has a higher CFM than another constellation for a fixed modulation order, it usually performs better. The CFM expression can be represented as follows:

$$CFM\left(C\right)=\frac{d_{min}^2}{P_{avg}}$$

where $d_{\min}$ – minimum Euclidean distance between characters, P_{avg} – average symbol power.

2.1.2 Peak to average power ratio (PAPR)

The average APSK symbol energy Es and the peak-to-average power ratio PAPR can be calculated as follows:

$$E_s=\frac{1}{M}\sum_{k=1}^{M}(s_{k,I}^2+s_{k,Q}^2)$$

$$PAPR=\frac{P_{peak}}{P_{avg}}=\frac{\max\limits_{k\in[1,M]}\left(s_{k,I}^2+s_{k,Q}^2\right)}{\frac{1}{M}\sum_{k=1}^{M}(s_{k,I}^2+s_{k,Q}^2)}$$

where $S_{k,I}$ и $S_{k,Q}$ – in-phase and quadrature components of the k-th symbol in the signal constellation, M – total number of symbols (constellation positionality).

2.1.3 SEP - Symbol error probability

To compare constellations with different geometric arrangements of symbols on a 2D plane based on energy efficiency, it is reasonable to use the dependence of the symbol error probability (SEP) on the signal-to-noise ratio (SNR). The SEP value does not depend on the coding type or bit distribution by symbols; it only reflects the geometry of the signal constellation. According to the known SEP, the probability of bit error for a particular coding scheme can easily be calculated.

2.2 IHQAM and CTQAM

Existing constellation shaping methods can be divided into two categories: geometric constellation shaping (GS) and probabilistic constellation shaping (PS). In this paper, we analyze geometric approaches to constellation shaping, in which the arrangement of symbols on the complex plane is optimized to achieve more compact constellation shapes, or to simplify the symbol demodulation operation. We will assume that in the wireless communication system before transmission is carried out scrambling operation of the bit stream, so the transmitted bits and symbols are equally likely. Then, when using the maximum likelihood (ML) detection criterion for reception, the boundaries of decision making about the symbol value will be defined by Voronoi cells as decision regions.

Let us analyze and compare the performance of IHQAM and CTQAM. It should be noted that the parametric quadrature amplitude modulation θ-QAM when increasing the number of symbols does not form a circular constellation [11]. Based on the location of the constellation points, HQAM constellations are categorized into regular and irregular HQAM structures. Constellations for regular HQAM (RHQAM) are symmetric about the origin and have a square or cruciform shape [10, 22]. In IHQAM, the symmetry constraint is relaxed and the constellations tend to be circular as the modulation order M increases [10, 23].

An algorithm for forming IHQAM constellations from R-HQAM constellations is presented in [10]. CTQAM signals can be constructed via an iterative process that rearranges the signal points of M-ary regular HQAM according to the algorithm in [14]. Figure 1 shows the constructed CTQAM and IHQAM constellations for different values of M, demonstrating that they do not coincide.

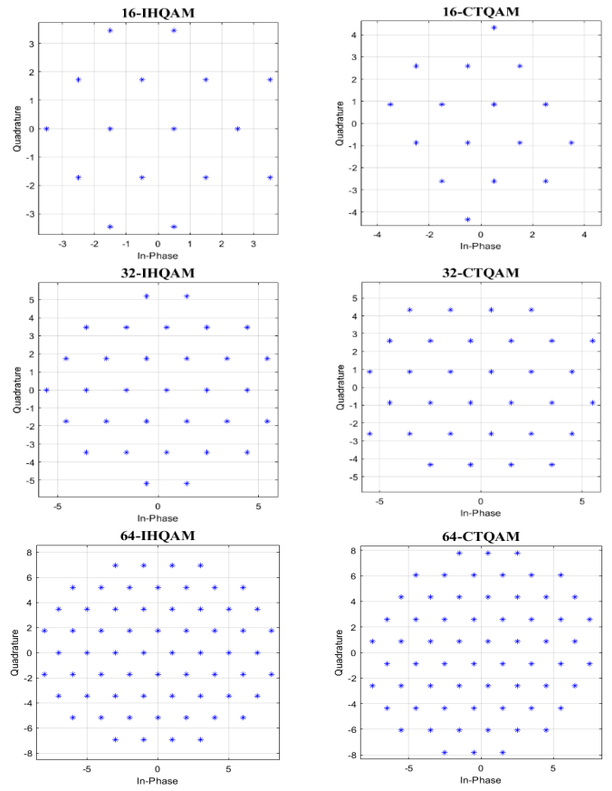

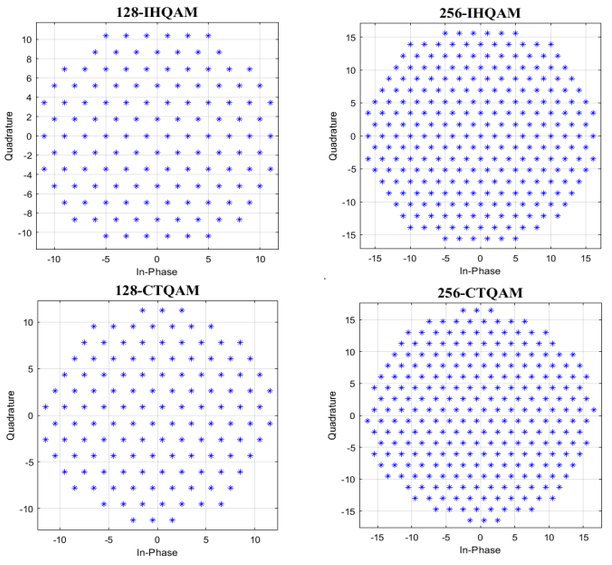

Fig. 1. IHQAM and CTQAM signal constellations for different M

2.2.1 Average symbol energy and peak-to-average power ratio for IHQAM and CTQAM

In IHQAM and CTQAM signals, all nearest neighbors of a signal point in the constellation are equidistant. Let d denote half of the minimum Euclidean distance between neighboring symbols in the constellation d_{min}=2d.

Let us calculate the average energy per symbol E_S and PAPR for IHQAM. The obtained values of E_S and PAPR are summarized in Table 1.

Table 1

Average symbol energy and PAPR of M-ary IHQAM

M	16	32	64	128	256
E_s / d^2	8.75	17.59	35.25	70.75	141
PAPR	1.742	1.879	1.9007	1.9699	2.03

In the case of CTQAM, the average symbol energy and PAPR for CTQAM at fixed minimum Euclidean distance can be expected to decrease because in the proposed construction method, a signal point of larger magnitude is rearranged into a new signal point of smaller magnitude, which causes the signal grouping of M-ary CTQAM to become circular as M increases. The E_S and PAPR values of the CTQAM are given in Table 2.

Table 2

Average symbol energy and PAPR of M-ary CTQAM

M	16	32	64	128	256
E_s / d^2	9	17.75	35.25	70.65	141.2
PAPR	2.111	2.0845	1.9007	1.9699	1.9757

For a two-dimensional signal constellation, the symbol error probability (SEP) depends primarily on the minimum distance between neighboring constellation points and the average symbol energy. As seen in the table, the average symbol energy for the IHQAM and CTQAM constellations is defined as $E_s = d^2 \cdot B$, where B is a constant depending on M. Let us define some parameters to simplify and reduce the expressions for the symbol error probability (SEP) obtained below. Since the signal-to-noise ratio for a symbol can be written as $\gamma = \frac{E_s}{N_0}$, where No/2 denotes the bilateral AWGN power spectral density with zero mean and $\sigma^2 = No/2$ denotes the noise variance, we introduce the normalized shortest distance (in noise standard deviations) from the signal point to the decision boundary. This distance is defined by the following expression: $\beta = \frac{d}{\sqrt{2N_o}}$, and expresses the symbolic signal-to-noise ratio through the value β.

$$\gamma = \frac{E_s}{N_0} = \frac{E_s}{2\sigma^2} = \frac{E_s}{2d^2} \cdot \left(\frac{2d}{2\sigma}\right)^2 = \frac{E_s}{2d^2} \cdot (\beta)^2$$

where $\beta = \frac{2d}{2\sigma} = \frac{d}{\sigma} = \sqrt{\frac{\gamma}{E_s / 2d^2}}$.

The SEP expressions obtained further in this section will be functions of β.

2.2.2 Symbol error probabilities for IHQAM and CTQAM signals

Using the techniques proposed in [24, 25], we obtain analytical expressions for the symbolic error. This technique allows us to derive the simplest expressions for the symbol error probability (SEP), which use the one-dimensional Gaussian Q-function.

$$Q(x) = \frac{1}{\sqrt{2\pi}} \int_x^\infty exp\left(\frac{-t^2}{2}\right) dt$$

First, consider the IHQAM signals. Figure 2 illustrates the partitioning of the 16-IHQAM signal space into decision regions (Voronoi cells). The dots in the figure represent symbols, and the lines represent decision boundaries.

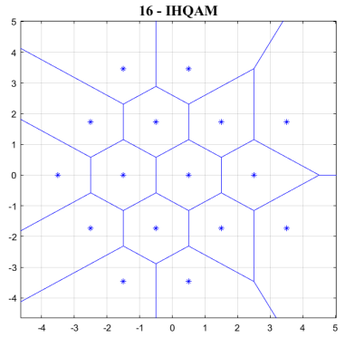

Fig. 2. Simplified detection method for 16-IHQAM constellation

The decision regions for inner symbols are closed, while those for edge symbols are semi-infinite. There are five types of signal points in this constellation, depending on each point's number of nearest neighbors. S_N - the number of signal points having N nearest neighbors, in terms of possible errors in determining the meaning of the symbol. There can be a total of five such points: S_2, S_3, S_4, S_5, S_6.

The probability of correctly receiving a symbol $P_{C,N}$ with N nearest neighbors is written as [24]

$$P_{C,2} = \left(1-Q(\beta)\right)^2 = 1-2Q(\beta)+Q(\beta)^2,$$

$$P_{C,3} = \left(1-Q(\beta)\right)^3 = 1-3Q(\beta)+3Q(\beta)^2-Q(\beta)^3,$$

$$P_{C,4} = \left(1-Q(\beta)\right)^4 = 1-4Q(\beta)+6Q(\beta)^2-4Q(\beta)^3+Q(\beta)^4$$

$$P_{C,5} = \left(1-Q(\beta)\right)^5 = 1-5Q(\beta)+10Q(\beta)^2-10Q(\beta)^3+5Q(\beta)^4-Q(\beta)^5,$$

$$P_{C,6} = \left(1-Q(\beta)\right)^6 = 1-6Q(\beta)+15Q(\beta)^2-20Q(\beta)^3$$
$$+15Q(\beta)^4-6Q(\beta)^5+Q(\beta)^6$$

where Q(β) - Gaussian Q-function.

Then the exact probability of correctly receiving a symbol for M-ary IHQAM and CTQAM is defined as [24]:

$$P_C(\beta) = \frac{1}{M}\left[S_2P_{C,2}+S_3P_{C,3}+S_4P_{C,4}+S_5P_{C,5}+S_6P_{C,6}\right]$$

where S_N – the number of signal points having N nearest neighbors.

a) IHQAM

The number of signal points having N nearest neighbors for M-ary IHQAM is given in Table 3.

Table 3

The number of signal points having N nearest neighbors for M-ary IHQAM

M	S_2	S_3	S_4	S_5	S_6
16	2	5	2	3	4
32	0	11	2	5	14
64	0	12	8	6	38
128	0	15	15	8	90
256	0	15	30	9	202

Therefore, the symbolic error, calculated as $P_e(\beta) = 1-P_C(\beta)$, will be written as:

$$P_e(\beta) = A_1Q(\beta)-A_2Q(\beta)^2+A_3Q(\beta)^3-A_4Q(\beta)^4$$
$$+A_5Q(\beta)^5-A_6Q(\beta)^6 \quad (1)$$

Table 4 summarizes A_N and β coefficients for different M:

Table 4

A_N and β coefficients for different M for M-ary IHQAM

M	16	32	64	128	256
β	$\sqrt{\frac{\gamma}{4.375}}$	$\sqrt{\frac{\gamma}{8.795}}$	$\sqrt{\frac{\gamma}{17.625}}$	$\sqrt{\frac{\gamma}{35.375}}$	$\sqrt{\frac{\gamma}{70.5}}$
A_1	4.125	4.6875	5.0937	5.3515	5.5546
A_2	7.4375	9.5312	11.1562	12.2265	13.0664
A_3	7.6875	10.9062	13.5000	15.2734	16.7773
A_4	4.8125	7.4062	9.5000	10.9765	12.1289
A_5	1.6875	2.7812	3.6562	4.2812	4.7695
A_6	0.2500	0.4375	0.5937	0.7031	0.7890

Equation (1) gives us an accurate, easy-to-calculate value for the SEP of M-ary IHQAM in the presence of AWGN channel.

Computer simulations were performed to verify the accuracy of the obtained expressions. Figure 3 shows the SEP plots of 16-, 32-, 64-, 128-, and 256-IHQAM signals. The simulation results show good agreement with the values calculated using the above formulas.

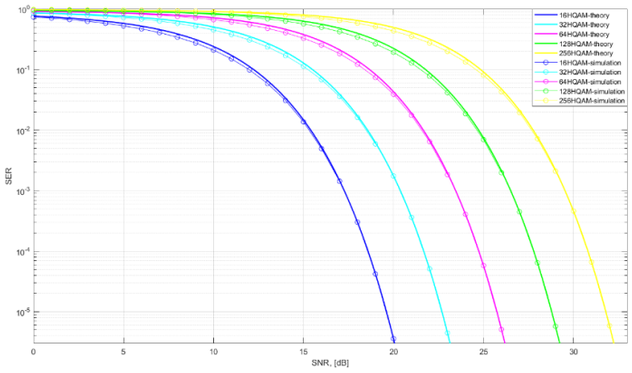

Fig. 3. SEP of M-ary irregular HQAM in AWGN channel *CTQAM*

The CTQAM symbol error probability will be determined by the methodology used in the case of irregular HQAM. Table 5 shows the number of nearest neighbors for M-ary CTQAM, where S_N - the number of signal points having N nearest neighbors.

Table 5

The number of signal points having N nearest neighbors for M-ary CTQAM

M	S_2	S_3	S_4	S_5	S_6
16	2	4	4	2	4
32	2	6	6	4	14
64	0	12	8	6	38
128	0	14	16	8	90
256	0	20	22	14	200

Then SEP for CTQAM signals can be written as:

$$P_e(\beta) = A_1Q(\beta)-A_2Q(\beta)^2+A_3Q(\beta)^3-A_4Q(\beta)^4$$
$$+A_5Q(\beta)^5-A_6Q(\beta)^6 \quad (2)$$

where A_N and β coefficients for different M are summarized in Table 6:

Table 6

A_N and β coefficients for different M for M-ary CTQAM

M	16	32	64	128	256
β	$\sqrt{\frac{\gamma}{4.5}}$	$\sqrt{\frac{\gamma}{8.875}}$	$\sqrt{\frac{\gamma}{17.625}}$	$\sqrt{\frac{\gamma}{35.28}}$	$\sqrt{\frac{\gamma}{70.6}}$
A_1	4.1250	4.6875	5.0937	5.3594	5.5390
A_2	7.3750	9.5625	11.1562	12.2500	13.0156
A_3	7.5000	10.9375	13.5000	15.2968	16.5937
A_4	4.6250	7.3750	9.5000	10.9843	12.0781
A_5	1.6250	2.7500	3.6562	4.2812	4.7421
A_6	0.2500	0.4375	0.5937	0.7031	0.7812

To verify the validity of the obtained expression (2), computer modeling was performed. The results of the SEP calculation

with simulation and calculations according to formula (2) for different modulation orders depending on the symbol signal-to-noise ratio are shown in figure 4. A good agreement between the theory and the simulation results can be observed.

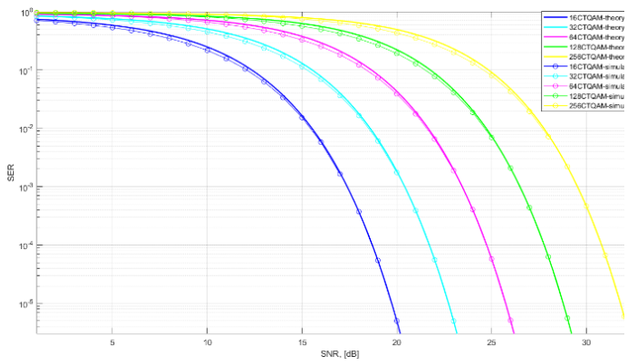

Fig. 4. SEP of M-ary CTQAM in AWGN channel

2.3 APSK signals of the Digital Video Broadcast System (DVB) S2X standard [16, 17]

Modulation schemes describing APSK constellations have the following form: $(n_1+n_2+\ldots+n_m)$ APSK, m – the total number of circles in the constellation, a n_i – the number of symbols on the i-th ring (circle). We can denote the ratio of the radius of the (i+1)-th ring to the radius of the first ring as $\gamma_i=R_{i+1}/R_1$. Different values of the radius coefficients γ_i are used to optimize transmission channel capacity with different signal-code constructions.

2.3.1 Average symbol energy and peak-to-average power ratio of APSK modulation power

The general formulas for calculating E_S and PAPR of DVB S2X standard can be represented as follows:

$$E_s = \frac{1}{M}\left(n_0 + n_1\gamma_1 + n_2\gamma_2 + \cdots\right)\cdot R_1^2 = \frac{1}{M}\left(n_0 + \sum_{i=1}^{N} n_i\gamma_i^2\right)R_1^2$$

$$PAPR = \frac{R_{max}^2}{\frac{1}{M}\left(n_0 + n_1\gamma_1 + n_2\gamma_2 + \cdots\right)\cdot R_1^2} = \frac{M\cdot\gamma_N^2}{n_0 + \sum_{i=1}^{N} n_i\gamma_i^2}$$

where $N+1$ – the total number of circles in the constellation, n_i – number of symbols on the i-th ring of the constellation, $M = \sum_{l=1}^{N+1} n_l$ – total number of symbols.

2.3.2 Estimates of symbol error probability of DVB S2X standard APSK signals

We will use the methods proposed in [26, 27] to obtain analytical expressions for estimating the symbol error probability of DVB-S2X standard APSK signals. As is known [28], the upper bound of SEP at M-ary modulation is given in the form of:

$$P(E) = \frac{1}{M}\sum_{i=1}^{M} P(E|s_i) \le \frac{1}{M}\sum_{i=1}^{M}\sum_{j=1, j\neq i}^{M} P\left(s_i \to s_j\right) \qquad (3)$$

where E denotes the error event, $P(E|s_i)$ – error probability at transmission of the i-th symbol, $P\left(s_i \to s_j\right)$ – denotes the pair-wise probability that a transmitted symbol Si is erroneously detected as s_j and M denotes the order of the constellation. The pair-wise probability can be computed using the Q-function, expressed in terms of the Euclidean distance d_{ij} and the single-sided noise spectral density No, as:

$$P\left(s_i \to s_j\right) = Q\left(d_{ij} / \sqrt{2N_0}\right)$$

However, calculations using formula (3) require finding error probabilities for all symbols of the constellation, which becomes very cumbersome as the order of the constellation increases. Considering the APSK symmetry of the constellation, [26] propose considering only the signal points of the first quarter. Thus, determining the SEP requires considering only one-fourth of the symbols and generalizing the obtained expressions to the entire constellation.

Despite the reduction in computational costs, obtaining analytical SEP expressions remains quite complex when the modulation order is large. To simplify PS estimation, we propose a technique that uses Voronoi diagrams to construct the constellations under study in [27]. This technique simplifies calculations when the symbols in the APSK constellation rings are uniformly distributed. When applying the maximum likelihood (ML) detection criterion for symbol detection, which involves scrambling the bitstream before modulation so that the transmitted symbols are considered equally likely, the Voronoi cells set the boundaries of the decision regions according to the value of the received symbol. As shown in [27], the decision boundaries between different APSK constellation rings can be approximated by concentric circles. When all symbols in each APSK constellation ring are uniformly distributed, the error detection probabilities are equal for all symbols in the ring. Additionally, the symbols in a ring are equidistant from the circular decision boundary that separates them from symbols in a neighboring ring. Therefore, calculating the pairwise error probability of one symbol per ring suffices to approximate the error characteristics of APSK schemes.

Consequently, the pair-wise error probability of a single symbol per ring is sufficient to approximate the error performance of APSK schemes.

Based on this, an expression for the SEP calculation containing a limited number of symbols equal to the number of rings in the constellation is derived in [27]:

$$P(E)_{APSK} = \frac{1}{m}\sum_{l=1}^{N} P(E|s_k)\cdot n_l \qquad l = 1 \ldots N$$

where N – total number of rings in the constellation, n_l denotes the number of symbols on the l-th ring in one quadrant of the constellation, $m = \sum_{l}^{N} n_l$, k denotes the subscript of the character, and $P(E|s_k)$ denotes the pair-wise probability for the k-th symbol.

In the future, we will use the methods described above to find analytical expressions of the symbolic errors of modulation schemes with arbitrary circular constellations, considering the peculiarities of the constellations.

16-APSK DVB S2X [17]

The 16-APSK constellations resemble two circles, one with a radius of R_1 and the other with a radius of R_2 (8+8) APSK, and they are described by two modulation schemes shown in Figures 5a and 5b. We can denote the ratio of the outer and inner radii as $\gamma_1 = R_2/R_1$, γ_1 takes the value $\gamma_1 = 2{,}19$. The decision areas for the accepted symbol values by the maximum likelihood (ML) criterion are presented in Figures 5c and 5d.

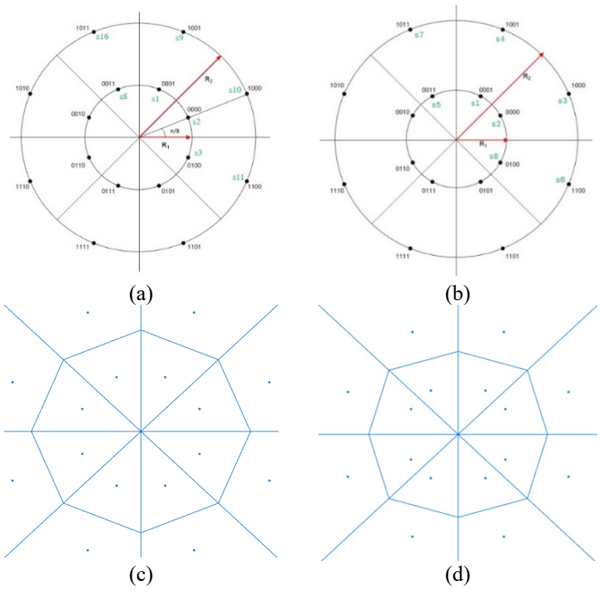

Fig. 5. Constellation diagrams for 16-APSK (a) code rate 90/180 and code rate 18/30 (b). Decision domains for the meaning of accepted symbols for 16-APSK (c) code rate 90/180 and code rate 18/30 (d)

8+8-APSK (code rate 90/180)

The average symbol energy for 16-APSK satisfies the ratio:

$$E_s = \left(2R_1^2 + 2R_2^2\right)/4 = R_1^2\left(1+\gamma^2\right)/2$$

Specifically, we derive the symbol error expression using the technique in [25]. The 16-APSK modulation's symbol error probability (SEP) can be written as follows, using the symmetry in the constellation shown in Figure 5:

$$P(E) = \frac{1}{4}\left\{P(E|s_1) + P(E|s_9) + P(E|s_2) + P(E|s_{10})\right\} \qquad (4)$$

First, let us consider obtaining an upper bound on $P(E|s_1)$. Since s_1 can be erroneously defined for any of the remaining 15 symbols, the union bound, which includes the corresponding 15 pairwise error terms, is given as follows:

$$P(E|s_1) \le \sum_{i=2}^{16} P(s_1 \to s_i)$$

However, the above expression includes significant overlaps in the error detection region, increasing the difference between the bound and the actual error rate. Including three pairwise error terms for symbols s_2, s_8, and s_9 is sufficient to obtain the upper bound since adding any other term creates redundant error regions. Thus, we obtain:

$$P(E|s_1) \le P(s_1 \to s_2) + P(s_1 \to s_8) + P(s_1 \to s_9) \qquad (5)$$

Similarly, we can verify that including the three pairwise probabilistic error terms for $P(E|s_9), P(E|s_2)$ and $P(E|s_{10})$ is sufficient:

$$\begin{aligned} P(E|s_2) &\le P(s_2 \to s_1) + P(s_2 \to s_3) + P(s_2 \to s_{10}) \\ P(E|s_9) &\le P(s_9 \to s_{16}) + P(s_9 \to s_{10}) + P(s_9 \to s_1) \\ P(E|s_{10}) &\le P(s_{10} \to s_9) + P(s_{10} \to s_{11}) + P(s_{10} \to s_2) \end{aligned} \qquad (6)$$

Combining equations (5) and (6) into (4), SEP for 16-APSK, reduces to the form:

$$P(E) \le \frac{1}{4}\left\{4Q\left(\frac{d_{1,2}}{\sqrt{2N_0}}\right) + 2Q\left(\frac{d_{9,10}}{\sqrt{2N_0}}\right) + 4Q\left(\frac{d_{1,9}}{\sqrt{2\ \ _0}}\right)\right\}$$

From the geometry of the 16-APSK constellation, it can be shown that the Euclidean distances between symbols are satisfied.

$$d_{1,9} = d_{2,10} = R_2 - R_1;\ d_{1,2} = 2R_1 sin\left(\frac{\pi}{8}\right);\ d_{9,10} = 2R_2 sin\left(\frac{\pi}{8}\right)$$

We obtain the final expression for SEP estimation by expressing the distances between symbols through the average symbol energy.

$$P(E) \le Q\left(\sqrt{\frac{E_s}{N_0}\frac{2-\sqrt{2}}{1+\gamma^2}}\right) + Q\left(\sqrt{\frac{E_s}{N_0}\frac{(\gamma-1)^2}{1+\gamma^2}}\right) + \frac{1}{2}Q\left(\sqrt{\frac{E_s}{N_0}\frac{\left(2-\sqrt{2}\right)\gamma^2}{1+\gamma^2}}\right)$$

8+8-APSK (code rate 18/30)

The average symbol energy for 16-APSK satisfies the ratio:

$$E_s = \left(2R_1^2 + 2R_2^2\right)/4 = R_1^2\left(1+\gamma^2\right)/2$$

Using the symmetry in the constellation shown in figure 5, the SEP of the 16-APSK modulation can be written as:

$$P(E) = \frac{1}{4}\left\{P(E|s_1) + P(E|s_2) + P(E|s_3) + P(E|s\ )\right\}$$

Consider the necessary error events for the selected symbols, as well as the corresponding Euclidean distances between the symbols obtained from the constellation geometry:

$$d_{1,2} = \sqrt{R_1^2\left(2-\sqrt{3}\right)};\ d_{1,5} = R_1;$$

$$d_{1,4} = \sqrt{R_1^2 + R_2^2 - 2R_1R_2cos\left(\frac{\pi}{24}\right)};\ d_{3,6} = \sqrt{R_2^2\left(2-\sqrt{2}\right)}$$

After some transformations we obtain the following expression of SEP dependence on SNR and constellation parameters:

$$P(E) \le \frac{1}{2}\cdot Q\left(\sqrt{\frac{E_s}{N_0}\cdot\frac{2-\sqrt{3}}{1+\gamma^2}}\right)+\frac{1}{2}\cdot Q\left(\sqrt{\frac{E_s}{N_0}\cdot\frac{1}{1+\gamma^2}}\right)$$

$$+Q\left(\sqrt{\frac{E_s}{N_0}\cdot\frac{\left(2-\sqrt{2}\right)\gamma^2}{1+\gamma^2}}\right)+Q\left(\sqrt{\frac{E_s}{N_0}\cdot\frac{1+\gamma^2-2\gamma cos\left(\frac{\pi}{24}\right)}{1+\gamma^2}}\right)$$

32-APSK DVB S2X

The 32-APSK uses two modulation schemes. The first scheme has four points on the first ring, twelve on the second ring, and sixteen on the third ring (4+12+16). The second scheme has four rings with four points on the first ring, eight on the second, four on the third, and sixteen on the fourth (4+8+4+16). The two schemes are shown in Figure 6(a) and 6(b).

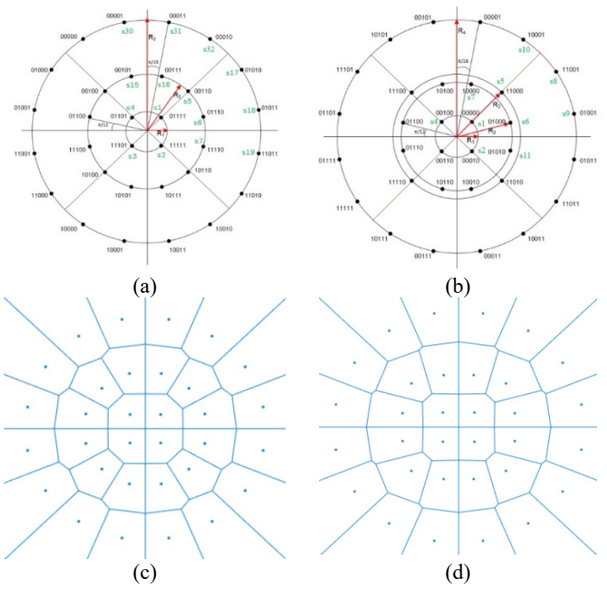

Fig. 6. Constellation diagrams for 4+12+16-APSK (a) and 4+8+4+16-APSK (b). Decision domains for the meaning of accepted symbols for 4+12+16-APSK (c) and 4+8+4+16-APSK (d)

4+12+16-APSK

32-APSK DVB S2X standard of 4+12+16-APSK type (Fig. 6) defines the value of radius coefficients $\gamma_1 = 2.84$ and γ_2 (5.26; 5.55).

The average symbol energy for 32-APSK satisfies the relation:

$$E_s = \left(4R_1^2+12R_2^2+16R_3\right)/32 = R_1^2\left(1+3\gamma_1^2+4\gamma_2^2\right)/8 = R_1^2\alpha/8$$

where $\alpha = \left(1+3\gamma_1^2+4\gamma_2^2\right)$.

The 32-APSK modulation in constellation SEP can be written using symmetry as follows:

$$P(E) = \frac{1}{8}\left\{\begin{matrix} P(E|s_1)+P(E|s_5)+2P(E|s_6) \\ +2P(E|s_{18})+2P(E|s_{17}) \end{matrix}\right\}$$

Describe the necessary error events for the selected symbols $P(E|s_1)$, $P(E|s_5)$, $P(E|s_{18})$ *and* $P(E|s_{17})$ and consider the corresponding Euclidean distances between the symbols:

$$d_{1,2} = d_{1,4} = R_1\sqrt{2};\ d_{1,5} = R_2 - R_1;$$

$$d_{1,6} = d_{1,16} = \sqrt{R_1^2+R_2^2-R_1R_2\sqrt{3}};$$

$$d_{5,6} = d_{5,16} = 2sin\left(\frac{\pi}{12}\right)R_2;\ d_{17,18} = d_{17,32} = 2sin\left(\frac{\pi}{16}\right)R_3;$$

$$d_{6,18} = \sqrt{R_2^2+R_3^2-2R_2R_3cos\left(\frac{\pi}{48}\right)};$$

$$d_{5,17} = d_{5,32} = \sqrt{R_2^2+R_3^2-2R_2R_3cos\left(\frac{\pi}{16}\right)};$$

$$d_{6,19} = \sqrt{R_2^2+R_3^2-2R_2R_3cos\left(\frac{7\pi}{18}\right)};$$

$$d_{5,18} = d_{5,31} = \sqrt{R_2^2+R_3^2-2R_2R_3cos\left(\frac{3\pi}{16}\right)};$$

$$d_{6,17} = \sqrt{R_2^2+R_3^2-2R_2R_3cos\left(\frac{5\pi}{48}\right)};$$

We obtained the analytical dependence of SEP on the signal-to-noise ratio (SNR).

$$P(E) \le \frac{1}{4}Q\left(\sqrt{\frac{E_S}{N_0}\cdot\frac{8}{\alpha}}\right)+\frac{1}{4}Q\left(\sqrt{\frac{E_S}{N_0}\cdot\frac{4\left(1+\gamma_1^2-\gamma_1\right)}{\alpha}}\right)$$

$$+\frac{1}{2}Q\left(\sqrt{\frac{E_S}{N_0}\cdot\frac{\left(\gamma_1^2-1\right)^2}{\alpha}}\right)+\frac{3}{4}Q\left(\sqrt{\frac{E_S}{N_0}\cdot\frac{16\sin\left(\frac{\pi}{12}\right)^2\gamma_1^2}{\alpha}}\right)$$

$$+\frac{5}{4}Q\left(\sqrt{\frac{E_S}{N_0}\cdot\frac{4\left(\gamma_2^2+\gamma_1^2-2\gamma_1\gamma_2\cos\frac{\pi}{16}\right)}{\alpha}}\right)$$

$$+Q\left(\sqrt{\frac{E_S}{N_0}\cdot\frac{16\sin\left(\frac{\pi}{16}\right)^2\gamma_2^2}{\alpha}}\right)$$

$$+\frac{1}{2}Q\left(\sqrt{\frac{E_S}{N_0}\cdot\frac{4\left(\gamma_2^2+\gamma_1^2-2\gamma_1\gamma_2\cos\frac{5\pi}{48}\right)}{\alpha}}\right)$$

4+8+4+16-APSK

4+8+4+4+16-APSK DVB S2X standard is shown in figure 4, the values of coefficients lie in the range of γ_1 (2.6; 2.8); γ_2 (2.86; 3.08) and $\gamma_3 = 5.6$ [17].

The average symbol energy for 32-APSK satisfies the relation

$$E_s = R_1^2\left(1+2\gamma_1^2+\gamma_2^2+4\gamma_3^2\right)/8 = R_1^2\alpha/8$$

where $\alpha = \left(1+2\gamma_1^2+\gamma_2^2+4\gamma_3^2\right)$.

Using the symmetry in the constellation shown in figure 4, the SEP of the 32-APSK modulation can be written as:

$$P(E) = \frac{1}{8}\left\{P(E|s_1)+P(E|s_5)+2P(E|s_6)+4P(E|s_8)\right\}$$

Computing the Euclidean distances between symbols derived from constellation geometry:

$$d_{1,2} = R_1\sqrt{2};\ d_{6,7} = R_2;$$

$$d_{1,6} = d_{1,16} = \sqrt{R_1^2+R_2^2-2R_1R_2\cos\left(\frac{\pi}{6}\right)};$$

$$d_{6,11} = \sqrt{R_2^2\left(2-\sqrt{3}\right)};$$

$$d_{5,7} = \sqrt{R_2^2+R_3^2-2R_2R_3\cos\left(\frac{\pi}{6}\right)};$$

$$d_{5,8} = \sqrt{R_3^2+R_4^2-2R_4R_3\cos\left(\frac{\pi}{16}\right)};$$

$$d_{8,9} = \sqrt{2R_4^2\left(1-\cos\left(\frac{\pi}{8}\right)\right)}$$

Expressing the distances between symbols through the average symbol energy, we obtain the final expression for SEP estimation in the form:

$$P(E) \le \frac{1}{4}Q\left(\sqrt{\frac{E_s}{N_0}\cdot\frac{8}{\alpha}}\right)+\frac{1}{4}Q\left(\sqrt{\frac{E_s}{N_0}\cdot\frac{4\cdot\gamma_1^2}{\alpha}}\right)$$
$$+\frac{1}{4}Q\left(\sqrt{\frac{E_s}{N_0}\cdot\frac{4\left(2-\sqrt{3}\right)\gamma_1^2}{\alpha}}\right)+\frac{1}{2}Q\left(\sqrt{\frac{E_s}{N_0}\cdot\frac{4\left(1+\gamma_1^2-\gamma_1\sqrt{3}\right)}{\alpha}}\right)$$
$$+\frac{1}{2}Q\left(\sqrt{\frac{E_s}{N_0}\cdot\frac{4\left(\gamma_2^2+\gamma_1^2-\gamma_1\gamma_2\sqrt{3}\right)}{\alpha}}\right)+Q\left(\sqrt{\frac{E_s}{N_0}\cdot\frac{8\left(1-\cos\frac{\pi}{8}\right)\gamma_3^2}{\alpha}}\right)$$
$$+\frac{3}{4}Q\left(\sqrt{\frac{E_s}{N_0}\cdot\frac{4\left(\gamma_2^2+\gamma_3^2-2\gamma_3\gamma_2\cos\frac{\pi}{16}\right)}{\alpha}}\right)$$

64-APSK DVB S2X

Three different 64-APSK constellations are introduced, the first with 16 points on the first ring, 16 on the second ring, 16 on the third ring and 16 on the fourth ring (16+16+16+16), the second with 8 points on the first ring, 16 on the second ring, 20 on the third ring and 20 on the fourth ring (8+16+20+20), the third with 4 points on the first ring, 12 on the second ring, 20 on the third ring and 28 on the fourth ring (4+12+20+28). The three schemes are shown in figure 7a, 8a, and 9a, respectively.

16+16+16+16-APSK

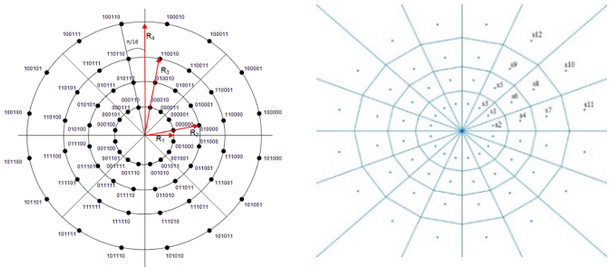

(a) (b)

Fig. 7. Constellation diagrams for 16+16+16+16-APSK (a). Decision domains for the meaning of accepted symbols for 16+16+16+16-APSK (b)

The radius ratio coefficients are γ_1 = 1,88; γ_2 = 2,72 and γ_3 = 3,95.

The average symbol energy of the constellation is given in the form:

$$E_s = \left(16R_1^2+16R_2^2+16R_3+16R_4^2\right)/64$$
$$= R_1^2\left(1+\gamma_1^2+\gamma_2^2+\gamma_3^2\right)/4 = R_1^2\alpha/4$$

where $\alpha = \left(1+\gamma_1^2+\gamma_2^2+\gamma_3\right)$.

Using the method proposed in [27] the symbol error probability can be written as:

$$P(E) = \frac{1}{16}\sum_{l=1}^{4}P(E|s_k)\cdot n_l$$
$$= \frac{1}{16}\left\{4P(E|s_1)+4P(E|s_6)+4P(E|s_8)+4P(E|s_{10})\right\}$$

Euclidean distances between symbols in the constellation:

$$d_{1,3} = d_{1,2} = 2sin\left(\frac{\pi}{32}\right)R_1;\ d_{6,5} = d_{6,4} = 2sin\left(\frac{\pi}{32}\right)R_2;$$

$$d_{8,9} = d_{8,7} = 2sin\left(\frac{\pi}{32}\right)R_3;\ d_{10,12} = d_{10,11} = 2sin\left(\frac{\pi}{32}\right)R_4;$$

$$d_{1,6} = R_2 - R_1;\ d_{6,8} = R_3 - R_2;\ d_{8,10} = R_4 - R_3;$$

After several transformations, we obtain the following expression for the SEP:

$$P(E) \le \frac{1}{2}Q\left(\beta\cdot\sqrt{\frac{E_s}{N_0}}\right)+\frac{1}{2}Q\left(\gamma_1\beta\cdot\sqrt{\frac{E_s}{N_0}}\right)$$
$$+\frac{1}{2}Q\left(\gamma_2\beta\cdot\sqrt{\frac{E_s}{N_0}}\right)+\frac{1}{2}Q\left(\gamma_3\beta\cdot\sqrt{\frac{E_s}{N_0}}\right)$$
$$+\frac{1}{4}Q\left(\sqrt{\frac{E_s}{N_0}\cdot\frac{2(\gamma_1-1)^2}{\alpha}}\right)+\frac{1}{2}Q\left(\sqrt{\frac{E_s}{N_0}\cdot\frac{2(\gamma_2-\gamma_1)^2}{\alpha}}\right)$$
$$+\frac{1}{4}Q\left(\sqrt{\frac{E_s}{N_0}\cdot\frac{2(\gamma_3-\gamma_2)^2}{\alpha}}\right)$$

4+12+20+28 APSK

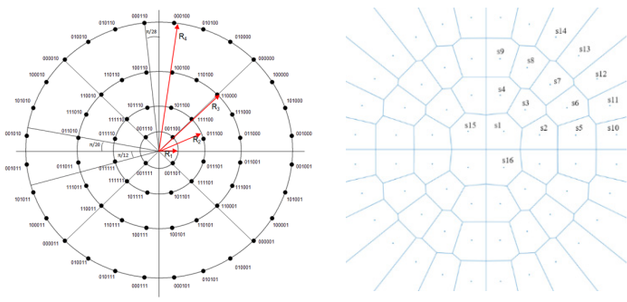

(a) (b)

Fig. 8. Constellation diagrams for 4+12+20+28-APSK (a). Decision domains for the meaning of accepted symbols for 4+12+20+28-APSK (b)

The radius ratio coefficients are $\gamma_1 = 2{,}4$; $\gamma_2 = 4{,}3$ and $\gamma_3 = 7$.

The average symbol energy of the constellation is given in the form:

$$E_s = \left(4R_1^2 + 12R_2^2 + 20R_3^2 + 28R_4^2\right)/64$$

$$= R_1^2\left(1 + 3\gamma_1^2 + 5\gamma_2^2 + 7\gamma_3^2\right)/16 = R_1^2\alpha$$

where $\alpha = \left(1 + 3\gamma_1^2 + 5\gamma_2^2 + 7\gamma_3^2\right)/16$

The probability of a symbol error can be expressed as follows:

$$P(E) = \frac{1}{16}\sum_{l=1}^{4} P(E|s_k)\cdot n_l$$

$$= \frac{1}{16}\left\{P(E|s_1) + 3P(E|s_3) + 5P(E|s_7) + 7P(E|s_{13})\right\}$$

Given the distances between characters:

$$d_{1,2} = \sqrt{R_1^2 + R_2^2 - 2R_1R_2\cos\left(\frac{\pi}{6}\right)};\ d_{3,7} = R_3 - R_2;\ d_{1,3} = R_2 - R_1$$

$$d_{7,13} = R_4 - R_3;\ d_{1,15} = R_1\sqrt{2};\ d_{3,2} = 2\sin\left(\frac{\pi}{12}\right)R_2;$$

$$d_{7,6} = 2\sin\left(\frac{\pi}{20}\right)R_3;\ d_{13,12} = 2\sin\left(\frac{\pi}{28}\right)R_4;$$

we obtain an expression for the symbolic error:

8+16+20+20-APSK

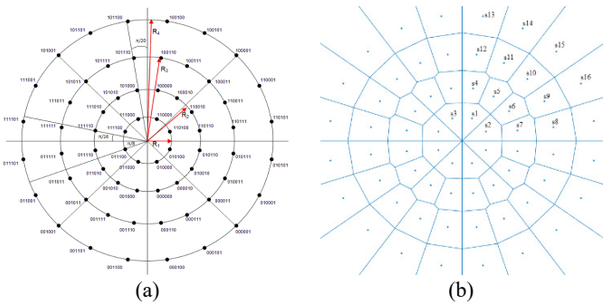

(a) (b)

Fig. 9. Constellation diagrams for 8+16+20+20-APSK (a). Decision domains for the meaning of accepted symbols for 8+16+20+20-APSK (b)

The values of coefficients lie in the range of $\gamma_1 = 2{,}2$; γ_2 (3,5; 3,6) and γ_3(5,2; 5,0) [17]

The average symbol energy of the constellation is given in the form:

$$E_s = \left(8R_1^2 + 16R_2^2 + 20R_3^2 + 20R_4\right)/64$$

$$= R_1^2\left(1 + 2\gamma_1^2 + \frac{5}{2}\gamma_2^2 + \frac{5}{2}\gamma_3\right)/8 = R_1^2\alpha/8$$

where $\alpha = \left(1 + 2\gamma_1^2 + \frac{5}{2}\gamma_2^2 + \frac{5}{2}\gamma_3\right)$

The upper bound of SEP can be represented as:

$$P(E) = \frac{1}{16}\sum_{l=1}^{4} P(E|s_k)\cdot n_l$$

$$= \frac{1}{16}\left\{2P(E|s_1) + 4P(E|s_5) + 5P(E|s_{11}) + 5P(E|s_{14})\right\}$$

Describing the necessary error events for the selected symbols $P(E|s_1)$, $P(E|s_5)$, $P(E|s_{11})$, $P(E|s_{14})$ and considering the corresponding Euclidean distances between the symbols:

$$d_{1,2} = \sqrt{R_1^2\left(2 - \sqrt{2}\right)};$$

$$d_{1,4} = d_{1,5} = \sqrt{R_1^2 + R_2^2 - 2R_1R_2\cos\left(\frac{\pi}{16}\right)};$$

$$d_{5,6} = \sqrt{2R_2^2\left(1 - \cos\left(\frac{\pi}{8}\right)\right)};$$

$$d_{5,11} = \sqrt{R_2^2 + R_3^2 - 2R_2R_3\cos\left(\frac{3\pi}{80}\right)};$$

$$d_{10,11} = \sqrt{2R_3^2\left(1 - \cos\left(\frac{\pi}{10}\right)\right)};\ d_{11,14} = R_4 - R_3;$$

$$d_{14,15} = \sqrt{2R_4^2\left(1 - \cos\left(\frac{\pi}{10}\right)\right)}$$

The upper bound of SEP as a function of $\frac{E_s}{N_0}$ can be written as follows:

$$P(E) \le \frac{1}{4}Q\left(\sqrt{\frac{E_s}{N_0}\cdot\frac{4\left(2-\sqrt{2}\right)}{\alpha}}\right) + \frac{1}{2}Q\left(\sqrt{\frac{E_s}{N_0}\cdot\frac{8\left(1-\cos\frac{\pi}{8}\right)\gamma_1^2}{\alpha}}\right)$$

$$+\frac{5}{8}Q\left(\sqrt{\frac{E_s}{N_0}\cdot\frac{4\left(\gamma_3-\gamma_2\right)^2}{\alpha}}\right) + \frac{9}{16}Q\left(\sqrt{\frac{E_s}{N_0}\cdot\frac{4\left(\gamma_2^2+\gamma_1^2-2\gamma_1\gamma_2\cos\frac{3\pi}{80}\right)}{\alpha}}\right)$$

$$+\frac{5}{8}Q\left(\sqrt{\frac{E_s}{N_0}\cdot\frac{8\left(1-\cos\frac{\pi}{10}\right)\gamma_2^2}{\alpha}}\right) + \frac{5}{8}Q\left(\sqrt{\frac{E_s}{N_0}\cdot\frac{8\left(1-\cos\frac{\pi}{10}\right)\gamma_3^2}{\alpha}}\right)$$

$$+\frac{1}{2}Q\left(\sqrt{\frac{E_s}{N_0}\cdot\frac{4\left(1+\gamma_1^2-2\gamma_1\cos\frac{\pi}{10}\right)}{\alpha}}\right)$$

128-APSK DVB S2X

Figure 10 shows that 128-APSK is characterized by six constellation rings with 16, 16, 16, 16, 16 and 48 evenly spaced PSK constellation points, respectively, with radii R_1, R_2, R_3, R_4, R_5, and R_6.

The radius ratio coefficients are γ_1= 1,715; γ_2= 2,118; γ_3= 2,681; γ_4= 2,75; γ_5= 3,733 and 3,819 [17]. The average symbolic energy of the constellation is given in the form:

$$E_s = \left(16R_1^2 + 16R_2^2 + 16R_3^2 + 16R_4^2 + 16R_5 + 48R_6^2\right)/128$$
$$= R_1^2\left(1+\gamma_1^2+\gamma_2^2+\gamma_3^2+\gamma_4^2+3\gamma_5^2\right)/8 = R_1^2\alpha/8,$$

where $\alpha = \left(1+\gamma_1^2+\gamma_2^2+\gamma_3+\gamma_4+3\gamma_5^2\right)$.

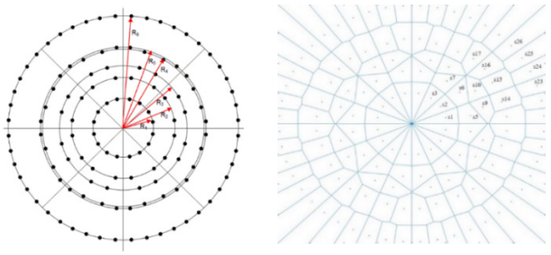

(a) (b)

Fig. 10. Constellation diagrams for 128-APSK (a). Decision domains for the meaning of accepted symbols for 128-APSK (b)

Applying the method proposed in [26] to 128-APSK, the symbol error probability can be written as:

$$P(E) = \frac{1}{8}\left\{\begin{matrix} P(E|s_2)+P(E|s_6)+P(E|s_{10})+P(E|s_{15}) \\ +P(E|s_{16})+P(E|s_{24})+P(E|s_{25})+P(E|s_{26}) \end{matrix}\right\}$$

Describing the necessary error events for the selected symbols and considering the corresponding Euclidean distances between the symbols obtained from the constellation geometry:

$$d_{1,2} = \sqrt{2R_1^2\left(1-cos\left(\frac{\pi}{8}\right)\right)};$$

$$d_{2,6} = \sqrt{R_1^2+R_2^2-2R_1R_2cos\left(\frac{\pi}{56}\right)};$$

$$d_{6,7} = \sqrt{2R_2^2\left(1-cos\left(\frac{97\pi}{1008}\right)\right)};$$

$$d_{6,5} = \sqrt{2R_2^2\left(1-cos\left(\frac{155\pi}{1008}\right)\right)};$$

$$d_{6,10} = \sqrt{R_3^2+R_2^2-2R_3R_2cos\left(\frac{43\pi}{1260}\right)};$$

$$d_{10,9} = \sqrt{2R_3^2\left(1-cos\left(\frac{431\pi}{5040}\right)\right)};$$

$$d_{10,15} = \sqrt{R_3^2+R_4^2-2R_3R_4cos\left(\frac{11\pi}{5040}\right)};$$

$$d_{14,15} = \sqrt{2R_4^2\left(1-cos\left(\frac{17\pi}{210}\right)\right)};$$

$$d_{16,17} = \sqrt{2R_5^2\left(1-cos\left(\frac{89\pi}{1680}\right)\right)};$$

$$d_{15,25} = \sqrt{R_4^2+R_6^2-2R_6R_4cos\left(\frac{19\pi}{1008}\right)};$$

$$d_{15,24} = \sqrt{R_4^2+R_6^2-2R_6R_4cos\left(\frac{17\pi}{840}\right)};$$

$$d_{24,25} = \sqrt{2R_6^2\left(1-cos\left(\frac{197\pi}{5040}\right)\right)};$$

$$d_{15,16} = \sqrt{R_5^2+R_4^2-2R_5R_4cos\left(\frac{73\pi}{1260}\right)};$$

$$d_{16,25} = \sqrt{R_5^2+R_6^2-2R_6R_5cos\left(\frac{197\pi}{5040}\right)}$$

$$d_{16,26} = \sqrt{R_5^2+R_6^2-2R_6R_5cos\left(\frac{23\pi}{5040}\right)};$$

$$d_{16,10} = \sqrt{R_5^2+R_3^2-2R_3R_5cos\left(\frac{281\pi}{5040}\right)}.$$

The probability of symbolic error can be written in the following form:

$$P(E) \le \frac{1}{4}Q\left(\sqrt{\frac{E_s}{N_0}\cdot\frac{8\left(1-\cos\frac{\pi}{8}\right)}{\alpha}}\right)+\frac{1}{4}Q\left(\sqrt{\frac{E_s}{N_0}\cdot\frac{4\left(1+\gamma_1^2-2\gamma_1\cos\frac{\pi}{56}\right)}{\alpha}}\right)$$
$$+\frac{1}{8}Q\left(\sqrt{\frac{E_s}{N_0}\cdot\frac{8\left(1-\cos\frac{97\pi}{1008}\right)\gamma_1^2}{\alpha}}\right)+\frac{1}{8}Q\left(\sqrt{\frac{E_s}{N_0}\cdot\frac{8\left(1-\cos\frac{155\pi}{1008}\right)\gamma_1^2}{\alpha}}\right)$$
$$+\frac{1}{8}Q\left(\sqrt{\frac{E_s}{N_0}\cdot\frac{8\left(1-\cos\frac{431\pi}{5040}\right)\gamma_2^2}{\alpha}}\right)+\frac{1}{8}Q\left(\sqrt{\frac{E_s}{N_0}\cdot\frac{8\left(1-\cos\frac{17\pi}{210}\right)\gamma_3^2}{\alpha}}\right)$$
$$+\frac{1}{8}Q\left(\sqrt{\frac{E_s}{N_0}\cdot\frac{8\left(1-\cos\frac{89\pi}{1680}\right)\gamma_4^2}{\alpha}}\right)+\frac{3}{4}Q\left(\sqrt{\frac{E_s}{N_0}\cdot\frac{8\left(1-\cos\frac{197\pi}{5040}\right)\gamma_5^2}{\alpha}}\right)$$
$$+\frac{1}{4}Q\left(\sqrt{\frac{E_s}{N_0}\cdot\frac{4\left(\gamma_2^2+\gamma_1^2-2\gamma_1\gamma_2\cos\frac{43\pi}{1260}\right)}{\alpha}}\right)+\frac{1}{4}Q\left(\sqrt{\frac{E_s}{N_0}\cdot\frac{4\left(\gamma_2^2+\gamma_3^2-2\gamma_3\gamma_2\cos\frac{11\pi}{5040}\right)}{\alpha}}\right)$$
$$+\frac{1}{4}Q\left(\sqrt{\frac{E_s}{N_0}\cdot\frac{4\left(\gamma_3^2+\gamma_4^2-2\gamma_3\gamma_4\cos\frac{73\pi}{1260}\right)}{\alpha}}\right)+\frac{1}{4}Q\left(\sqrt{\frac{E_s}{N_0}\cdot\frac{4\left(\gamma_3^2+\gamma_5^2-2\gamma_3\gamma_5\cos\frac{19\pi}{1008}\right)}{\alpha}}\right)$$
$$+\frac{1}{4}Q\left(\sqrt{\frac{E_s}{N_0}\cdot\frac{4\left(\gamma_3^2+\gamma_5^2-2\gamma_3\gamma_5\cos\frac{17\pi}{840}\right)}{\alpha}}\right)+\frac{1}{4}Q\left(\sqrt{\frac{E_s}{N_0}\cdot\frac{4\left(\gamma_4^2+\gamma_5^2-2\gamma_4\gamma_5\cos\frac{197\pi}{5040}\right)}{\alpha}}\right)$$
$$+\frac{1}{4}Q\left(\sqrt{\frac{E_s}{N_0}\cdot\frac{4\left(\gamma_4^2+\gamma_5^2-2\gamma_4\gamma_5\cos\frac{23\pi}{5040}\right)}{\alpha}}\right)$$
$$+\frac{1}{8}Q\left(\sqrt{\frac{E_s}{N_0}\cdot\frac{4\left(\gamma_2^2+\gamma_4^2-2\gamma_4\gamma_2\cos\frac{281\pi}{5040}\right)}{\alpha}}\right)$$

256-APSK DVB S2X

Consider a 256-APSK constellation with eight rings, each of which contains 32 evenly spaced symbols. Figure 11 shows a diagram of the signaling constellation and the decision region.

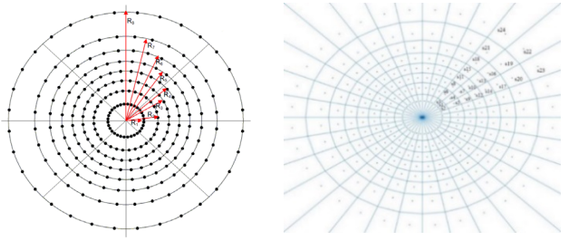

(a) (b)

Fig. 11. Constellation diagrams for 256-APSK (a). Decision domains for the meaning of accepted symbols for 256-APSK (b)

The values of coefficients lie in the range of γ_1(1,791; 1,794); γ_2(2,405; 2,409); γ_3(2,980; 2,986); γ_4(3,569; 3,579); γ_5(4,045; 4,235); γ_6(4,5; 5,078) and γ_7(5,4; 6,536). [17]

Denoting the radius ratios as γ_i, we write the average symbolic energy of the constellation in the form:

$$E_s = \frac{1}{8}\sum_{i=1}^{8} R_i^2 = \frac{1}{8}R_1^2\left(1+\sum_{i=1}^{7}\gamma_i^2\right) = \frac{1}{8}R_1^2\alpha,$$

where $\alpha = \left(1+\gamma_1^2+\gamma_2^2+\gamma_3+\gamma_4+\gamma_5+\gamma_6+\gamma_7\right)$

The probability of a symbol error can be written as:

$$P(E) = \frac{1}{64}\sum_{i=1}^{8} P(E|s_i)\cdot n_i$$

$$= \frac{1}{8}\left\{\begin{matrix} P(E|s_1)+P(E|s_4)+P(E|s_7)+P(E|s_{10}) \\ +P(E|s_{13})+P(E|s_{16})+P(E|s_{19})+P(E|s_{22}) \end{matrix}\right\}$$

Calculating geometrically Euclidean distances between constellation symbols:

$$d_{1,2} = 2sin\left(\frac{\pi}{32}\right)R_1;\ d_{4,5} = 2sin\left(\frac{\pi}{32}\right)R_2;\ d_{7,9} = 2sin\left(\frac{\pi}{32}\right)R_3;$$

$$d_{10,12} = 2sin\left(\frac{\pi}{32}\right)R_4;\ d_{13,14} = 2sin\left(\frac{\pi}{32}\right)R_5;$$

$$d_{16,17} = 2sin\left(\frac{\pi}{32}\right)R_6;$$

$$d_{19,20} = 2sin\left(\frac{\pi}{32}\right)R_7;\ d_{22,23} = 2sin\left(\frac{\pi}{32}\right)R_8;\ d_{1,4} = R_2 - R_1;$$

$$d_{4,7} = R_3 - R_2;\ d_{7,10} = R_4 - R_3;\ d_{10,13} = R_5 - R_4;$$

$$d_{13,16} = R_6 - R_5;\ d_{16,19} = R_7 - R_6;\ d_{22,19} = R_8 - R_7.$$

and expressing them through γ_i and SNR (E_S/N_0), we obtain an expression for the symbolic error estimation in the form of:

$$P(E) \le \frac{1}{4}\left[Q\left(\beta\cdot\sqrt{\frac{E_s}{N_0}}\right)+\sum_{i=1}^{7}Q\left(\gamma_i\beta\cdot\sqrt{\frac{E_s}{N_0}}\right)\right]$$

$$+\frac{1}{4}\left[\begin{matrix} \frac{1}{2}Q\left(\frac{2(\gamma_1-1)}{\sqrt{\alpha}}\cdot\sqrt{\frac{E_s}{N_0}}\right)+\frac{1}{4}Q\left(\frac{2(\gamma_2-\gamma_1)}{\sqrt{\alpha}}\cdot\sqrt{\frac{E_s}{N_0}}\right) \\ +\frac{1}{4}Q\left(\frac{2(\gamma_3-\gamma_2)}{\sqrt{\alpha}}\cdot\sqrt{\frac{E_s}{N_0}}\right)+\frac{1}{4}Q\left(\frac{2(\gamma_4-\gamma_3)}{\sqrt{\alpha}}\cdot\sqrt{\frac{E_s}{N_0}}\right) \\ +\frac{1}{4}Q\left(\frac{2(\gamma_5-\gamma_4)}{\sqrt{\alpha}}\cdot\sqrt{\frac{E_s}{N_0}}\right)+\frac{1}{4}Q\left(\frac{2(\gamma_6-\gamma_5)}{\sqrt{\alpha}}\cdot\sqrt{\frac{E_s}{N_0}}\right) \\ +\frac{1}{2}Q\left(\frac{2(\gamma_7-\gamma_6)}{\sqrt{\alpha}}\cdot\sqrt{\frac{E_s}{N_0}}\right) \end{matrix}\right]$$

where $\beta = \frac{4\sin\frac{\pi}{32}}{\sqrt{\alpha}}$

Computer modeling was performed to verify the accuracy of the obtained formulas. Figure 12 shows the SEP graphs obtained from the formulas and the modeling results, which demonstrate a high degree of consistency.

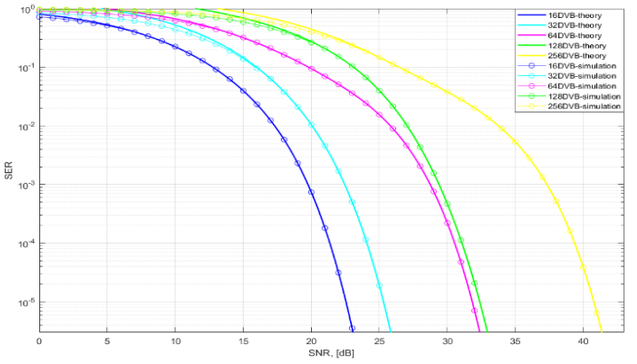

Fig. 12. SEP for DVB-S2X modulation schemes in channel AWGN

2.4 Signals standard MIL-STD-188-110

Let us analyze the APSK signals of the MIL-STD-188-110 standard. The constellations and the geometric relationships between symbols are shown in Fig. 13 [19], where the maximum signal amplitude is equal to one. As shown in the figure, the APSK constellations with M = 16, 32, and 64 symbols are formed by combining an S-QAM constellation (inner) with one or two M-PSK circles (outer). For M = 256, the constellation is "rounded" into a rectangular lattice by rearranging the symbols.

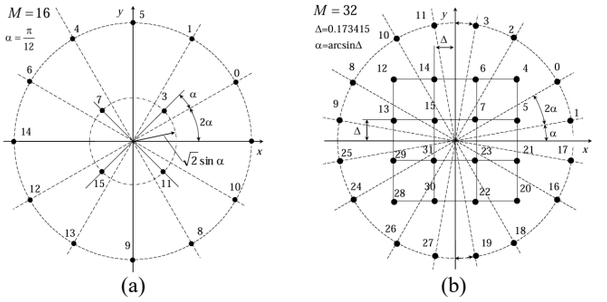

(a) (b)

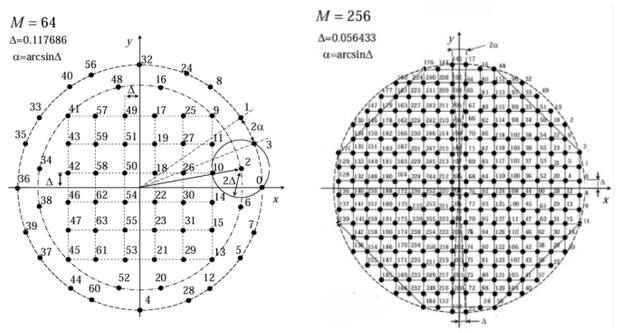

(c) (d)

Fig. 13. M-QAM constellations of MIL-STD-188-110 signals. M = 16 (a), M = 32 (b), M = 64 (c), M = 256 (d)

Let us determine the average symbol energy Es, and the peak-to-average power ratio (PAPR) for such signals. As figure 13(a) shows, the 16-QAM constellation consists of two PSK rings: an inner 4PSK ring and an outer 12PSK ring. The distance between the inner constellation points is $d_{min} = 2\Delta$, and at the maximum signal amplitude R=1, the distance between neighboring symbols of the outer ring is approximately Δ.The average energy of one symbol is $E_s = \frac{1}{4(2\Delta^2 + 3R^2)}$, Therefore, the expression for PAPR is $PAPR = \frac{4R^2}{2\Delta^2 + 3R^2}$.

The Constellation 32-QAM standard (MIL-STD-188-110) is a linear combination of the 16-S-QAM and 16-PSK constellations (see Fig. 13b). The outer symbols, which are located on a circle of radius R=1 are distributed so that the minimum distance between them is the minimum Euclidean distance, $d_{min} = 2\Delta$. Additionally, the minimum distance between the outer circle symbols and the 16-QAM symbols is 2Δ. The average symbol energy for this constellation is $E_s = \frac{1}{2(10\Delta^2 + R^2)}$. The expression for PAPR takes the form $PAPR = \frac{2R^2}{10\Delta^2 + R^2}$.

Constellation 64-QAM is a linear combination of 36-SQAM and the two circular constellations, 8-PSK and 20-PSK (see Fig. 13c). The points on the two outer circles are chosen to be distant by a minimum distance of 2Δ apart from each other and from the nearest points in the square part of the constellation. The radius of the inner circle is $R_1 = 5\sqrt{2}\Delta$, and the radius of the outer circle is R_2=1. Using the sum-of-squares formula for odd numbers $\sum_{n=1}^{N}(2n-1)^2 = \frac{N(2N-1)(2N+1)}{3}$ we can find the average symbol energy for this constellation $E_s = \frac{310\Delta^2 + 5R_2^2}{16}$ and $PAPR = \frac{16R_2^2}{310\Delta^2 + 5R_2^2}$.

The 256-QAM constellation is a "rounded" constellation obtained from the hexagon in figure 13d by adding points. By denoting the radius of the outer circle as R=1 and applying the formula for the sum of the squares of odd numbers to the columns of the constellation, we can derive the expression for the average symbol energy in terms of the magnitude of Δ and R

$$E_S = \frac{10126\Delta^2 + R^2}{64} \text{ and } PAPR = \frac{64R^2}{10126\Delta^2 + R^2}.$$

Table 7 shows the PAPR signal values and parameter Δ, which is equal to half the minimum Euclidean distance between the points d_{min}. It also shows the expressions for determining the PAPR signals for different M values at the maximum signal amplitude R=1.

Table 7

MIL-STD-188-110 M-QAM signal parameters

M	16	32	64	256
$\Delta = \frac{d_{min}}{2}$	$\sin\left(\frac{\pi}{12}\right)$	0.17341	0.117686	$\frac{1}{\sqrt{314}}$
PAPR	$\frac{4}{2\Delta^2 + 3}$	$\frac{2}{10\Delta^2 + 1}$	$\frac{16}{310\Delta^2 + 5}$	$\frac{64}{10126\Delta^2 + 1}$

Obtain analytical expressions to determine the upper bound on the symbol error probability of MIL-STD-188-110 standard signals. Figure 14 shows the partitioning of the signal space into ML decision regions using Voronoi cells for M = 16, 32, 64 and 256.

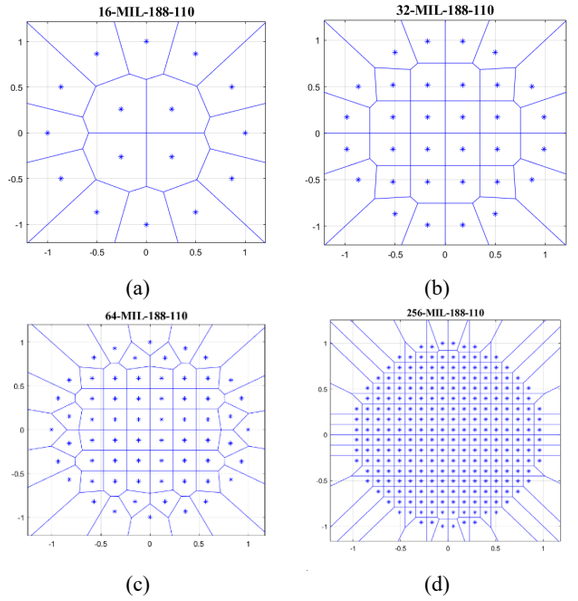

(a) (b)

(c) (d)

Fig. 14. Partitioning the M-QAM signal space of MIL-STD-188-110 signals into decision regions. M = 16 (a), M = 32 (b), M = 64 (c), M = 256 (d)

We will use the methodology applied earlier to derive analytical expressions for the symbol error of DVB-S2X standard APSK signals. After a number of transformations, the analytical expression of the symbol error probability (SEP) for a 16-QAM signal can be written as follows:

$$P(E) \le \frac{1}{4}\left\{\begin{array}{l} 4Q\left(\frac{d_{3,1}}{\sqrt{2N_0}}\right) + 2Q\left(\frac{d_{3,7}}{\sqrt{2N_0}}\right) \\ +6Q\left(\frac{d_{1,5}}{\sqrt{2N_0}}\right) + 2Q\left(\frac{d_{5,3}}{\sqrt{2N_0}}\right) \end{array}\right\}$$

where the distances between symbols are defined as:

$$d_{3,7} = 2\Delta;\ d_{3,1} = \sqrt{R^2 + 2\Delta^2 - 2\sqrt{2}\Delta R cos\left(\frac{\pi}{12}\right)}$$

$$d_{1,5} = R\sqrt{2 - 2cos\left(\frac{\pi}{6}\right)} = R\sqrt{2-\sqrt{3}};\ d_{5,3} = \sqrt{R^2 + 2\Delta^2 - 2\Delta R}$$

Unfortunately, since the MIL-STD-188-110 standard signals are not analytically described (defined by normalized constellations with fixed Δ and R values), there is no explicit dependence on the E_S/N_0. Ratio in the presented expression. Therefore, when carrying out calculations, it is convenient to fix the average energy of the E_S symbol at a given Δ and R while changing the power of the AWGN to obtain different SNR values.

An analytical SEP expression for the 32-QAM modulation is similarly derived:

$$P(E) \le \frac{3}{2}Q\left(\frac{d_{4,5}}{\sqrt{2N_o}}\right) + \frac{1}{4}Q\left(\frac{d_{0,2}}{\sqrt{2N_o}}\right) + \frac{1}{2}Q\left(\frac{d_{4,2}}{\sqrt{2N_o}}\right)$$
$$+\frac{1}{2}Q\left(\frac{d_{5,1}}{\sqrt{2N_o}}\right) + \frac{3}{4}Q\left(\frac{d_{1,0}}{\sqrt{2N_o}}\right) + \frac{1}{2}Q\left(\frac{d_{5,0}}{\sqrt{2N_o}}\right)$$

where the distances between symbols are defined as:

$$d_{4,5} = 2\Delta;\ d_{4,2} = \sqrt{R^2 + 18\Delta^2 - 6\sqrt{2}\Delta R cos\left(\frac{\pi}{12}\right)}$$

$$d_{1,0} = 2sin(\alpha);\ d_{0,2} = 2Rsin\left(\frac{3\alpha}{2}\right);$$

$$d_{5,1} = \sqrt{R^2 + 10\Delta^2 - 2\sqrt{10}\Delta R cos\left(arctg\left(\frac{1}{3}\right) - \alpha\right)};$$

$$d_{5,0} = \sqrt{R^2 + 10\Delta^2 - 2\sqrt{10}\Delta R cos\left(3\alpha - arctg\left(\frac{1}{3}\right)\right)}.$$

Using the same technique, the symbolic error is found for the 64-QAM case in the form:

$$P(E) \le \frac{11}{4}Q\left(\frac{d_{27,11}}{\sqrt{2N_o}}\right) + \frac{1}{4}Q\left(\frac{d_{1,11}}{\sqrt{2N_o}}\right) + \frac{1}{4}Q\left(\frac{d_{3,11}}{\sqrt{N_o}}\right)$$
$$+\frac{1}{4}Q\left(\frac{d_{9,1}}{\sqrt{2N_o}}\right) + \frac{1}{4}Q\left(\frac{d_{2,11}}{\sqrt{2N_o}}\right) + \frac{3}{8}Q\left(\frac{d_{3,0}}{\sqrt{2N_o}}\right)$$

where the distances between symbols are defined as:

$$d_{27,11} = 2\Delta;\ d_{3,0} = 2Rsin\left(\frac{\frac{\pi}{2} - 4\alpha}{6}\right);$$

$$d_{1,11} = \sqrt{R^2 + 34\Delta^2 - 2\sqrt{34}\Delta R cos\left(\frac{\frac{\pi}{2} + 2\alpha}{3} - arctg\left(\frac{3}{5}\right)\right)};$$

$$d_{3,11} = \sqrt{R^2 + 34\Delta^2 - 2\sqrt{34}\Delta R cos\left(arctg\left(\frac{3}{5}\right) - \frac{\frac{\pi}{2} - 4\alpha}{3}\right)};$$

$$d_{9,1} = \sqrt{R^2 + 50\Delta^2 - 2\sqrt{50}\Delta R cos\left(\frac{\pi}{4} - \frac{\frac{\pi}{2} + 2\alpha}{3}\right)};$$

$$d_{2,11} = R\sqrt{84\Delta^2 - 20\sqrt{17}\Delta^2 cos\left(arctg\left(\frac{3}{5}\right) - \frac{\frac{\pi}{2} - 4\alpha}{6}\right)}.$$

Finally, the SEP 256-QAM expression is as follows:

$$P(E) \le \frac{1}{64}\left[\begin{array}{l} 234Q\left(\frac{d_{68,84}}{\sqrt{2N_o}}\right) + 10Q\left(\frac{d_{6,3}}{\sqrt{2N_o}}\right) \\ +2Q\left(\frac{d_{64,17}}{\sqrt{2N_o}}\right) + 2Q\left(\frac{d_{16,17}}{\sqrt{2N_o}}\right) \end{array}\right]$$

where the distances between symbols are defined as:

$$d_{68,84} = 2\Delta;\ d_{6,3} = 2\sqrt{2}\Delta; d_{64,17} = R - 15\Delta;$$

$$d_{16,17} = \sqrt{(R - 17\Delta)^2 + 4\Delta^2}\ .$$

Computer modeling was carried out to check the accuracy of the obtained analytical expressions. Figure 15 shows plots of the SEP obtained by formulae and by simulation. The results show good agreement.

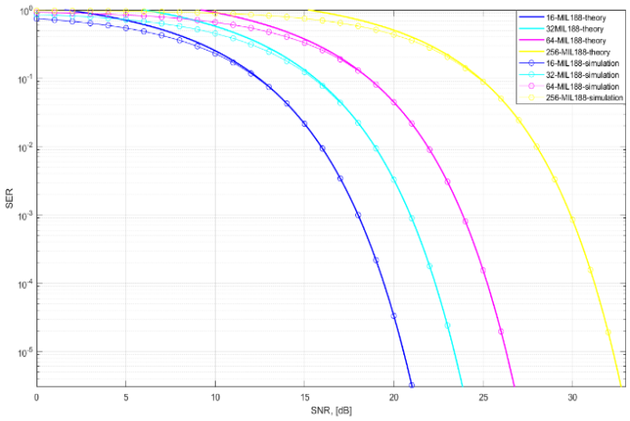

Fig. 15. SEP for MIL-STD-188-110 modulation schemes in channel AWGN

3 Discussions

Now, let's compare the studied APSK modulation schemes according to the selected performance criteria. Table 8 shows the PAPR and CFM values depending on the modulation order M. Figures 16 shows the symbol error characteristics obtained from SNR for different modulation types.

Table 8

The PAPR and CFM values depending on the modulation order

M	Modulation type		PAPR	$\frac{d_{min}^2}{E_s}$ (CFM)
16	DVB-S2X	8+8 APSK (code rate 90/180)	1,6549	0,202
		8+8 APSK (code rate 18/30)	1,6549	0,0924
	MIL-STD-188-110		1,304	0,3494
	IHQAM		1,742	0,457
	CTQAM		2,111	0,444
32	DVB-S2X	4+12+16APSK	1,6594	0,1081
		4+8+4+16 APSK	1,6849	0,1074
	MIL-STD-188-110		1,5376	0,1849
	IHQAM		1,879	0,2274
	CTQAM		2,0845	0,2253
64	DVB-S2X	16+16+16+16APSK	2,2665	0,0221
		4+12+20+28APSK	1,7279	0,0691
		8+16+20+20APSK	1,9545	0,04234
	MIL-STD-188-110		1,7216	0,09537
	IHQAM		1,9	0,1134
	CTQAM		1,9007	0,1134
128	DVB-S2X		1,7432	0,01819
	IHQAM		1,9699	0,0565
	CTQAM		1,9699	0,0566
256	DVB-S2X		2,895	0,0026
	MIL-STD-188-110		1,9249	0,02452
	IHQAM		2,07	0,02836
	CTQAM		1,9757	0,02832

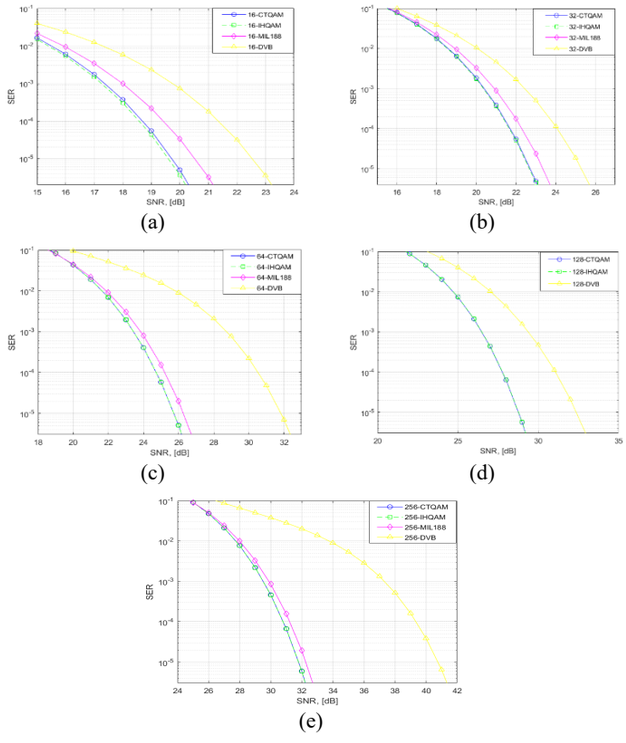

Fig. 16. SEP performance of the considered modulation schemes at fixed modulation order M. M = 16 (a), M = 32 (b), M = 64 (c), M = 128 (d), M = 256 (e)

As shown in Table 8, the signals of standard MIL-STD-188-110 have the smallest PAPR at fixed M and are slightly inferior to the IHQAM and CTQAM signals. The loss of IHQAM and CTQAM signals compared to the MIL-STD-188-110 standard significantly decreases with increasing modulation order, and at M = 256, their peak factors are nearly identical. The DVB-S2X standard has the worst PAPR and CFM characteristics. Only the 4+12+20+28-APSK and 128 APSK signals of the DVB-S2X standard have good PAPR characteristics.

Figure 16 shows graphs of SEP dependency on SNR for the considered modulation schemes at fixed modulation order values. According to these graphs, the signals with the lowest SEP values (the most energy efficient) are IHQAM and CTQAM. At SEP = 10^{-5} and M = 16 and 32, CTQAM loses to IHQAM by about 0.1 dB; however, at M ≥ 64, the SEP characteristics coincide. MIL-STD-188-110 signals are inferior to IHQAM and CTQAM signals by 1 dB at M = 16 and 0.5 dB at M = 256 at fixed SEP = 10^{-5}. DVB-S2X standard signals are significantly inferior to IHQAM and CTQAM signals by the SEP criterion. Thus, the smallest SNR loss is 3 dB at M = 16, increasing to 19 dB at M = 256.

The numerical values of the metrics calculated in this paper are in good agreement with the results of studies on the efficiency of HQAM and TQAM signals given in several published papers. [10,24,29]

Therefore, IHQAM and CTQAM signals have the best characteristics. Therefore, developing and realizing simple and fast algorithms for demodulating such signals is particularly relevant. It is also worth noting the quite good characteristics of MIL-STD-188-110 standard signals.

4 Conclusion

This paper presents a detailed study of the performance of various APSK modulation schemes with improved characteristics. These schemes may be of interest as candidates for use in high-speed, energy-efficient, high-capacity data transmission channels in modern and prospective wireless telecommunication networks.

Simple and accurate expressions were obtained for calculating the peak factor and symbol error probability of the compared constellations. The characteristics of IHQAM, CTQAM, and MIL-STD-188-110 and DVB-S2X signals were calculated and compared. The high efficiency and prospective use of the IHQAM, CTQAM, and MIL-STD-188-110 modulation schemes is proven.

The choice of a particular modulation scheme depends on the convenience of its use in specific wireless transmission technology. This depends on the characteristics of the transmission channel, spatial separation, MIMO technology, the use of RIS, and the ease and speed of modulation and demodulation algorithm realization.

Future research should more fully investigate the effectiveness of the considered modulation schemes under different multipath propagation channel models, nonlinear satellite channels, and other wireless info communication system application scenarios, including the use of multiple input, multiple output (MIMO) technology.

Acknowledgment

This research has been funded by the grant of the Russian Science Foundation (RSF), no. 25-21-00281, https://rscf.ru/en/project/25-21-00281/.

References

[1] M. D. Renzo, M. Debbah, D. T. Phan-Huy, *et al.*, "Smart radio environments empowered by reconfigurable AI meta-surfaces: An idea whose time has come," *EURASIP Journal on Wireless Communications and Networking*, vol. 2019, publication number 129, issue 1, pp. 129-138, 2019, doi: 10.1186/s13638-019-1438-9.

[2] M. Di Renzo, A. Zappone, M. Debbah, M. Alouini, C. Yuen, J. de Rosny, and S. Tretyakov, "Smart radio environments empowered by reconfigurable intelligent surfaces: How it works, state of research, and the road ahead," *IEEE Journal on Selected Areas in Communications*, vol. 38, no. 11, pp. 2450-2525, 2020, doi: 10.1109/JSAC.2020.3007211.

[3] W. Luo, T. Yan, A. Xuan, Y. Zhong, and X. Zhao, "Adaptive smart radio environment (ASRE): New paradigm for wireless communication networks," *IEEE Access*, vol. 12, pp. 12437-12445, 2024, doi: 10.1109/ACCESS.2024.3355140.

[4] M. S. B. Syed, H. M. Attaullah, S. Ali, and M. I. Aslam, "Wireless communications beyond antennas: The role of reconfigurable intelligent surfaces," *Engineering Proceedings*, 32 (1), 2023, doi: 10.3390/engproc2023032010.

[5] T. K. Oikonomou, D. Tyrovolas, and S. A. Tegos, "On the performance of RIS-assisted networks with HQAM," in *Proc. 2024 European Conf. Networks and Communications & 6G Summit (EuCNC & 6G Summit)*, Antwerp, Belgium, 2024, pp. 434-439, doi: 10.1109/EuCNC/6GSummit60053.2024.10597099.

[6] R. Samy, H. Yang, T. Rakia, and M. Alouini, "Parallel FSO-RF transmissions for high-throughput remote access with satellite communications," *IEEE Transactions on Aerospace and Electronic Systems*, vol. 59, no. 6, pp. 9417-9426, 2023, doi: 10.1109/TAES.2023.3319304.

[7] A. B. Wondmagen, D. S. Lakew, A. T. Tran, J. Paek, and S. Cho, "A review on FSO/RF based satellite-aerial-ground communication systems," in *Proc. 2024 Int. Conf. Information Networking (ICOIN)*, Ho Chi Minh City, Vietnam, 2024, pp. 421-425, doi: 10.1109/ICOIN59985.2024.10572075.

[8] Q. Sun, H. Qi, Y. Wang, X. Chen, J. Zhang, and M. Lopez, "Performance analysis of mixed FSO/RF system for satellite-terrestrial relay network," *IEEE Transactions on Vehicular Technology*, vol. 73, no. 8, pp. 11378-11393, 2024, doi: 10.1109/TVT.2024.3373653.

[9] G. Alnwaimi and H. Boujemaa, "Hybrid RF/FSO communications through reconfigurable intelligent surfaces in the presence of pointing errors," *Telecommunication Systems*, vol. 78, pp. 155-162, 2021, doi: 10.1007/s11235-021-00802-0.

[10] P. K. Singya, P. Shaik, N. Kumar, V. Bhatia, and M.-S. Alouini, "A survey on higher-order QAM constellations: Technical challenges, recent advances, and future trends," *IEEE Open Journal of the Communications Society*, vol. 2, pp. 617-655, 2021, doi: 10.1109/OJCOMS.2021.306738.

[11] K. N. Pappi, A. S. Lioumpas, and G. K. Karagiannidis, "θ-QAM: A parametric quadrature amplitude modulation family and its performance in AWGN and fading channels," *IEEE Transactions on Communications*, vol. 58, no. 4, pp. 1014-1019, 2010, doi: 10.1109/TCOMM.2010.04.080552.

[12] G. Foschini, R. Gitlin, and S. Weinstein, "Optimization of two-dimensional signal constellations in the presence of Gaussian noise," *IEEE Transactions on Communications*, vol. 22, no. 1, pp. 28-38, 1974, doi: 10.1109/TCOM.1974.1092061.

[13] A. Omidi, M. Zeng, J. Lin, and L. A. Rusch, "Geometric constellation shaping using initialized autoencoders," in *Proc. 2021 IEEE Int. Black Sea Conf. Communications and Networking (BlackSeaCom)*, Bucharest, Romania, 2021, pp. 1-5, doi: 10.1109/BlackSeaCom52164.2021.9527735.

[14] S. Ahn and D. Yoon, "Circular θ-QAM: A circle-shaped QAM for higher-order modulation," *IEEE Access*, vol. 7, pp. 149005-149012, 2019, doi: 10.1109/ACCESS.2019.2946339.

[15] P. K. Singya, N. Kumar, V. Bhatia, and M.-S. Alouini, "On the performance analysis of higher order QAM schemes over mixed RF/FSO systems," *IEEE Transactions on Vehicular Technology*, vol. 69, no. 7, pp. 7366-7378, 2020, doi: 10.1109/TVT.2020.2990747.

[16] ETSI EN 302 307-1 V1.4.1, "Digital Video Broadcasting (DVB); Second generation framing structure, channel coding and modulation systems for Broadcasting, Interactive Services, News Gathering and other broadband satellite applications," *European Telecommunications Standards Institute (ETSI)*, Jul. 2014.

[17] DVB Project, *Second generation framing structure, channel coding and modulation systems for broadcasting, interactive services, news gathering and other broadband satellite applications – Part 2: DVB-S2 extensions (DVB-S2X)*, DVB BlueBook A083-2, Feb. 2020.

[18] U.S. Department of Defense, *MIL-STD-188-110C: Interoperability and Performance Standards for Data Modems*, 2011.

[19] A. V. Petrov, V. V. Mikhalev, and A. A. Klyuev, "An algorithm for computing the bit-error rate in data transmission channels using two-dimensional signal-code constructions in the presence of signal-like jamming," *Systems of Control, Communication and Security*, no. 3, pp. 1-37, 2021, doi: 10.24412/2410-9916-2021-3-1-37.

[20] G. D. Forney and L. F. Wei, "Multidimensional constellations – Part I: Introduction, figures of merit, and generalized cross constellations," *IEEE Journal on Selected Areas in Communications*, vol. 7, no. 6, pp. 877-892, 1989, doi: 10.1109/49.2961.

[21] F. Cogen and E. Aydin, "Performance analysis of hexagonal QAM constellations on quadrature spatial modulation with perfect and imperfect channel estimation," *Physical Communication*, vol. 47, publication number 101379, 2021, doi: 10.1016/j.phycom.2021.101379.

[22] S.-J. Park, M.-K. Byeon, and J.-H. Jeon, "Odd-bit triangular quadrature amplitude modulations," in *Proc. IEEE 20th Int. Symp. Personal, Indoor and Mobile Radio Communications (PIMRC)*, Tokyo, Japan, 2009, pp. 2419-2423, doi: 10.1109/PIMRC.2009.5450367.

[23] S.-J. Park and M.-K. Byeon, "Irregularly distributed triangular quadrature amplitude modulation," in *Proc. IEEE 19th Int. Symp. Personal, Indoor and Mobile Radio Communications (PIMRC)*, Cannes, France, 2008, pp. 1-5, doi: 10.1109/PIMRC.2008.4699450.

[24] F. H. Qureshi, S. A. Sheikh, Q. U. Khan, and F. M. Malik, "SEP performance of triangular QAM with MRC spatial diversity over fading channels," *EURASIP Journal on Wireless Communications and Networking*, vol. 2016, no. 5, pp. 1-16, 2016, doi: 10.1186/s13638-015-0511-2.

[25] X. Zhang, H. Yu, and G. Wei, "Exact symbol error probability of cross-QAM in AWGN and fading channels," *EURASIP Journal on Wireless Communications and Networking*, vol. 2010, Article ID 917954, 2010, doi: 10.1155/2010/917954.

[26] W. Sung, S. Kang, P. Kim, D.-I. Chang, and D.-J. Shin, "Performance analysis of APSK modulation for DVB-S2 transmission over nonlinear channels," *International Journal of Satellite Communications and Networking*, vol. 27, no. 6, pp. 295-311, 2009, doi: 10.1002/sat.938.

[27] O. Afelumo, A. B. Awoseyila, and B. G. Evans, "Simplified evaluation of APSK error performance," *Electronics Letters*, vol. 48, no. 14, pp. 886-888, 2012, doi: 10.1049/el.2012.1740.

[28] R. E. Ziemer and R. L. Peterson, *Introduction to Digital Communication*, 2nd ed. Englewood Cliffs, NJ, USA: Prentice-Hall, 2001, 905 p.

[29] T. K. Oikonomou, S. A. Tegos, D. Tyrovolas, P. D. Diamantoulakis, and G. K. Karagiannidis, "On the error analysis of hexagonal-QAM constellations," *IEEE Communications Letters*, vol. 26, no. 8, pp. 1764-1768, 2022, doi: 10.1109/LCOMM.2022.3179454.

СРАВНИТЕЛЬНЫЙ АНАЛИЗ ХАРАКТЕРИСТИК ПЕРСПЕКТИВНЫХ СХЕМ APSK В БЕСПРОВОДНЫХ ТЕЛЕКОММУНИКАЦИЯХ

Казаков Геннадий Николаевич, *Московский авиационный институт (национальный исследовательский университет), Москва, Россия,* ***jee2@mail.ru***

Нгуен Хю Тунг, *Московский авиационный институт (национальный исследовательский университет), Москва, Россия,* ***nguyenhuytung201@gmail.com***

Шевгунов Тимофей Яковлевич, *Московский авиационный институт (национальный исследовательский университет), Москва, Россия,* ***shevgunov@gmail.com***

Ефимов Евгений Николаевич, *Московский авиационный институт (национальный исследовательский университет), Москва, Россия,* ***omegatype@gmail.com***

Исследование выполнено за счет гранта Российского научного фонда №25-21-00281, https://rscf.ru/project/25-21-00281/

Аннотация

Растущие требования на использование высокоскоростных и энергоэффективных каналов передачи данных большой ёмкости в современных и перспективных телекоммуникационных сетях привели к возрастающему интересу к вопросам формирования и применения сигналов с новыми созвездиями. Сформулированы требования к форме сигнальных созвездий в связи с появлением новых технологий беспроводных телекоммуникаций. Выбраны перспективные варианты модуляционных схем APSK с круговыми сигнальными созвездиями, которые включают сигналы с нерегулярной hexagonal quadrature amplitude modulation (IHQAM), сигналы с circular ?-quadrature amplitude modulation (CTQAM), а также сигналы стандартов Digital Video Broadcast System (DVB) S2X и MIL-STD-188-110. Для сравнения эффективности APSK сигналов использовались три показателя: коэффициент качества созвездия (CFM), отношение пиковой к средней мощности (PAPR) и вероятность символьной ошибки (SEP). По выбранным метрикам получены аналитические выражения показателей качества изучаемых сигналов и проведен их численный расчет. Сформулированы рекомендации о целесообразности использования исследуемых сигналов с круговыми созвездиями в современных и перспективных беспроводных телекоммуникационных сетях. Чтобы показать правильность предложенных аналитических выражений, приведены некоторые результаты точного компьютерного моделирования.

Ключевые слова: *сигналы с круговыми сигнальными созвездиями, коэффициент качества созвездия (CFM), отношение пиковой мощности к средней (PAPR), вероятность символьной ошибки (SEP), нерегулярные HQAM (IHQAM), круговая ?-квадратурная амплитудная модуляция (CTQAM), Star QAM, сигналы стандарта MIL-STD-188-110*

Литература

1. *Renzo M. D., Debbah M., Phan-Huy D. T.*, et al., Smart radio environments empowered by reconfigurable AI meta-surfaces: An idea whose time has come // EURASIP Journal on Wireless Communications and Networking, vol. 2019, publication number 129, issue 1, pp. 129-138, 2019, doi: 10.1186/s13638-019-1438-9.

2. *Di Renz M., Zappone A., Debbah M., Alouini M., Yuen C., de Rosny J., Tretyakov S.* Smart radio environments empowered by reconfigurable intelligent surfaces: How it works, state of research, and the road ahead // IEEE Journal on Selected Areas in Communications, vol. 38, no. 11, pp. 2450-2525, 2020, doi: 10.1109/JSAC.2020.3007211.

3. *Luo W., Yan T., Xuan A., Zhong Y., Zhao X.* Adaptive smart radio environment (ASRE): New paradigm for wireless communication networks // IEEE Access, vol. 12, pp. 12437-12445, 2024, doi: 10.1109/ACCESS.2024.3355140.

4. *Syed M. S. B., Attaullah H. M., Ali S., Aslam M. I.* Wireless communications beyond antennas: The role of reconfigurable intelligent surfaces // Engineering Proceedings, 32 (1), 2023, doi: 10.3390/engproc2023032010.

5. *Oikonomou T. K., Tyrovolas D., Tegos S. A.* On the performance of RIS-assisted networks with HQAM // Proc. 2024 European Conf. Networks and Communications & 6G Summit (EuCNC & 6G Summit), Antwerp, Belgium, 2024, pp. 434-439, doi: 10.1109/EuCNC/6GSummit60053.2024.10597099.

6. *Samy R., Yang H., Rakia T., Alouini M.* Parallel FSO-RF transmissions for high-throughput remote access with satellite communications // IEEE Transactions on Aerospace and Electronic Systems, vol. 59, no. 6, pp. 9417-9426, 2023, doi: 10.1109/TAES.2023.3319304.

7. *Wondmagen A. B., Lakew D. S., Tran A. T., Paek J., Cho S.* A review on FSO/RF based satellite-aerial-ground communication systems // Proc. 2024 Int. Conf. Information Networking (ICOIN), Ho Chi Minh City, Vietnam, 2024, pp. 421-425, doi: 10.1109/ICOIN59985.2024.10572075.

8. *Sun Q., Qi H., Wang Y., Chen X., Zhang J., Lopez M.* Performance analysis of mixed FSO/RF system for satellite-terrestrial relay network // IEEE Transactions on Vehicular Technology, vol. 73, no. 8, pp. 11378-11393, 2024, doi: 10.1109/TVT.2024.3373653.

9. *Alnwaimi G., Boujemaa H.* Hybrid RF/FSO communications through reconfigurable intelligent surfaces in the presence of pointing errors // Telecommunication Systems, vol. 78, pp. 155-162, 2021, doi: 10.1007/s11235-021-00802-0.

10. *Singya P. K., Shaik P., Kumar N., Bhatia V., Alouini M.-S.* A survey on higher-order QAM constellations: Technical challenges, recent advances, and future trends // IEEE Open Journal of the Communications Society, vol. 2, pp. 617-655, 2021, doi: 10.1109/OJCOMS.2021.306738.

11. Pappi K. N., Lioumpas A. S. Karagiannidis G. K. θ-QAM: A parametric quadrature amplitude modulation family and its performance in AWGN and fading channels // IEEE Transactions on Communications, vol. 58, no. 4, pp. 1014-1019, 2010, doi: 10.1109/TCOMM.2010.04.080552.

12. *Foschini G., Gitlin R., Weinstein S.* Optimization of two-dimensional signal constellations in the presence of Gaussian noise // IEEE Transactions on Communications, vol. 22, no. 1, pp. 28-38, 1974, doi: 10.1109/TCOM.1974.1092061.

13. *Omidi A., Zeng M., Lin J., Rusch L. A.* Geometric constellation shaping using initialized autoencoders // Proc. 2021 IEEE Int. Black Sea Conf. Communications and Networking (BlackSeaCom), Bucharest, Romania, 2021, pp. 1-5, doi: 10.1109/BlackSeaCom52164.2021.9527735.

14. *Ahn S., Yoon D.* Circular θ-QAM: A circle-shaped QAM for higher-order modulation // IEEE Access, vol. 7, pp. 149005-149012, 2019, doi: 10.1109/ACCESS.2019.2946339.

15. *Singya, P. K., Kumar N., Bhatia V., Alouini M.-S.* On the performance analysis of higher order QAM schemes over mixed RF/FSO systems // IEEE Transactions on Vehicular Technology, vol. 69, no. 7, pp. 7366-7378, 2020, doi: 10.1109/TVT.2020.2990747.

16. ETSI EN 302 307-1 V1.4.1, Digital Video Broadcasting (DVB); Second generation framing structure, channel coding and modulation systems for Broadcasting, Interactive Services, News Gathering and other broadband satellite applications. European Telecommunications Standards Institute (ETSI), Jul. 2014.

17. DVB Project, Second generation framing structure, channel coding and modulation systems for broadcasting, interactive services, news gathering and other broadband satellite applications - Part 2: DVB-S2 extensions (DVB-S2X), DVB BlueBook A083-2, Feb. 2020.

18. U.S. Department of Defense, MIL-STD-188-110C: Interoperability and Performance Standards for Data Modems, 2011.

19. *Петров А. В., Михалёв В. В., и Клюев А. А.* Алгоритм расчета вероятности ошибочного приема бита в каналах передачи данных с двумерными сигнально-кодовыми конструкциями под воздействием сигналоподобных помех // Системы управления, связи и безопасности, № 3. С. 1-37, 2021, doi: 10.24412/2410-9916-2021-3-1-37.

20. *Forney G. D., Wei L. F.* Multidimensional constellations - Part I: Introduction, figures of merit, and generalized cross constellations // IEEE Journal on Selected Areas in Communications, vol. 7, no. 6, pp. 877-892, 1989, doi: 10.1109/49.2961.

21. *Cogen F., Aydin E.* Performance analysis of hexagonal QAM constellations on quadrature spatial modulation with perfect and imperfect channel estimation // Physical Communication, vol. 47, publication number 101379, 2021, doi: 10.1016/j.phycom.2021.101379.

22. *Park S.-J., Byeon M.-K., Jeon J.-H.* Odd-bit triangular quadrature amplitude modulations // Proc. IEEE 20th Int. Symp. Personal, Indoor and Mobile Radio Communications (PIMRC), Tokyo, Japan, 2009, pp. 2419-2423, doi: 10.1109/PIMRC.2009.5450367.

23. *Park S.-J., Byeon M.-K.* Irregularly distributed triangular quadrature amplitude modulation // Proc. IEEE 19th Int. Symp. Personal, Indoor and Mobile Radio Communications (PIMRC), Cannes, France, 2008, pp. 1-5, doi: 10.1109/PIMRC.2008.4699450.

24. *Qureshi F. H., Sheikh S. A., Khan Q. U., Malik F. M.* SEP performance of triangular QAM with MRC spatial diversity over fading channels // EURASIP Journal on Wireless Communications and Networking, vol. 2016, no. 5, pp. 1-16, 2016, doi: 10.1186/s13638-015-0511-2.

25. *Zhang X., Yu H., Wei G.* Exact symbol error probability of cross-QAM in AWGN and fading channels // EURASIP Journal on Wireless Communications and Networking, vol. 2010, Article ID 917954, 2010, doi: 10.1155/2010/917954.

26. *Sung W., Kang S., Kim P., Chang D.-I., Shin D.-J.* Performance analysis of APSK modulation for DVB-S2 transmission over nonlinear channels // International Journal of Satellite Communications and Networking, vol. 27, no. 6, pp. 295-311, 2009, doi: 10.1002/sat.938.

27. *Afelumo O., Awoseyila A. B., Evans B. G.* Simplified evaluation of APSK error performance // Electronics Letters, vol. 48, no. 14, pp. 886-888, 2012, doi: 10.1049/el.2012.1740.

28. *Ziemer R. E., Peterson R. L.* Introduction to Digital Communication, 2nd ed. Englewood Cliffs, NJ, USA: Prentice-Hall, 2001, 905 p.

29. *Oikonomou T. K., Tegos S. A., Tyrovolas D., Diamantoulakis P. D., Karagiannidis G. K.* On the error analysis of hexagonal-QAM constellations // IEEE Communications Letters, vol. 26, no. 8, pp. 1764-1768, 2022, doi: 10.1109/LCOMM.2022.3179454.